國 立 交 通 大 學

電機與控制工程學系

博 士 論 文

腦神經人機界面及應用

Neural Human Machine Interface and Its Applications

研 究 生： 柯 立 偉
指導教授： 林 進 燈 教授

中 華 民 國 九 十 六 年 九 月

腦神經人機界面及應用

Neural Human Machine Interface and Its Applications

研 究 生：柯立偉　　Student：Li-Wei Ko

指導教授：林進燈 博士　　Advisor：Dr. Chin-Teng Lin

國立交通大學

電機與控制工程學系

博士論文

A Dissertation

Submitted to Department of Electrical and Control Engineering

College of Electrical Engineering

National Chiao Tung University

in partial Fulfillment of the Requirements

for the Degree of

Doctor of Philosophy

in

Electrical and Control Engineering

September 2007

Hsinchu, Taiwan, Republic of China

中 華 民 國 九 十 六 年 九 月

腦神經人機界面及應用

研究生：柯立偉　　指導教授：林進燈　博士

國立交通大學　電機與控制工程學系　博士班

摘　要

近年來在醫學診斷和神經生物學研究中，腦電波訊號(Electroencephalogram, EEG)已成為非常有用的非侵入式生理訊號工具，主要因為它能在千分之一秒(milliseconds)的時間裡提供極高的生理訊號解析度，直接反映出細胞群體中動態的變化。在所有量測大腦造影的醫療工具中，量測腦電波訊號最不受任何限制，因為在量測過程中，受試者不需受到固定身體和保持頭不動等限制。然而，若將現今市面上的腦波監測系統應用到日常生活中卻會深深受到許多限制，例如：需在頭皮上塗抹導電膠才能量測腦電波訊號，系統缺乏高精確度的量測，即時訊號處理和有效去除雜訊等功能，皆是主要腦波監測系統的缺失。因此，為了解決這些缺失，本論文主要目的在開發，設計和測試一可直接應用於日常生活環境裡的腦神經人機界面，可讓使用者在日常生活的自然情況下方便使用生理訊號監測系統，即使是在多變的環境中做不同的工作任務，亦能直接擷取大腦活動變化。更重要的是，本論文為了探討此創新的移動式無線腦神經人機界面的應用，我們亦建構一環繞式虛擬實境動態駕駛環境，此環境可真實的模擬日常生活的駕駛情境，無論是應用於神經科學基礎研究上或是應用於日常生活中的警示提醒，皆能有效地測試此腦神經人機界面的效能。在本論文中，我們提出三個與日常生活相關的應用研究，但絕不僅侷限於這些而已，這三個研究分別為：(1) 在虛擬實境動態駕駛環境裡探討受試者駕車時的認知狀態的變化；(2) 探討利用聲音回饋來

維持駕駛員的精神狀態和注意力是否集中的腦神經變化；(3) 在虛擬實境動態駕駛環境裡探討動態刺激對身體感覺和知覺的腦神經變化。對目前許多探討複雜腦功能的研究來說，本論文探討的應用能在生活環境裡受限最小並提出許多重要新穎的發現，這些研究成果亦可有效提升正常人每天在反覆工作任務環境下的工作能力表現，也可應用於腦傷、生病或身體不健全等病人更細部的動態認知狀態研究。否則這些成果至今僅能請受試者來傳統腦波實驗室參與實驗，並要求受試者固定身體，頭不能亂動，眼睛不能亂瞄等限制受試者行為。一旦有了創新的可攜式無線腦神經人機界面，這些限制將能一一破除，我們相信這能為認知神經科學和人機界面互動等研究開啟另一新的頁章。

Neural Human Machine Interface and Its Applications

Student: Li-Wei Ko Advisor: Dr. Chin-Teng Lin

Department of Electrical and Control Engineering

National Chiao Tung University

Abstract

Electroencephalogram is a powerful non-invasive tool widely used by for both medical diagnosis and neurobiological research because it provides high temporal resolution in milliseconds which directly reflects the dynamics of the generating cell assemblies, and it is the only brain imaging modality that does not require the head/body to be fixed. However, the lack of availability of EEG monitoring system capable of high-definition recording, online signal processing and artifact cancellation, without use of conductive gels applied to the scalp, has long thwarted the applications of EEG monitoring in the workplace. This dissertation describes a design, development and testing of a neural human machine interface that allows assessment of brain activities of participants actively performing ordinary tasks in natural body positions and situations within a real operational environment. More importantly, this dissertation also discuss the implications of this innovative mobile wireless brain imaging technology in neuroscience and neuro-technology, through three sample studies: (1) cognitive-state monitoring of participants performing realistic driving tasks in the virtual-reality-based dynamic driving simulator; (2) the efficacy and neural correlates of auditory feedback delivered to participants to maintain

participants attention and alertness; (3) the neural correlates of kinesthetic sensation and perception in the dynamic driving simulator. Results of these studies provide many new insights into the understanding of complex brain functions of participants performing ordinary/routine tasks in a minimum constrained environment. These results also allow a better appreciation of the limitations of normal human performance in repetitive task environments, and may allow more detailed study of changes in cognitive dynamics in brain-damaged, diseased, or genetically abnormal individuals. Furthermore, these findings might be difficult, if ever possible, to obtain in a standard EEG laboratory where participants are asked to limit their eye blinks, teeth clinching, head/ body movements. We, thus, believe this work opens a new chapter in neuro-cognitive human-machine interface/interaction.

誌　　謝

此博士論文的完成，首先感謝指導教授 林進燈老師在我博士班二年級時鼓勵我轉往生醫工程領域發展，他認為生醫工程是下一世代的新興領域，未來將有無限發展空間，因此我選擇加入腦科學研究中心團隊。在過去兩年多研究期間，林進燈老師辛勤地對外為腦科學研究中心爭取許多豐富的研究資源和實驗環境，並利用閒暇時間從旁指導研究，加入腦中心的同時也因此認識許多國際，國內知名研究團隊，例如：UCSC 的劉文泰教授，NASA JPL 的方偉騏教授、UCSD 的鍾子平教授和段正仁博士，MPIB 的李淑珍博士等。

在此要特別感謝 UCSD 鍾子平教授，在我撰寫博士論文期間提供許多建議和校閱博士論文，並在口試前幾日不眠不休地指導我如何完整有條理的簡報，使我在眾多大師級的口試委員面前表現受肯定，將腦中心的研究向外宣傳發揚。亦感謝段正仁博士從旁給予研究上的協助，從實驗設計、實驗分析、實驗結果討論到如果撰寫論文，皆具專業的意見與想法。

在參與腦科學研究的兩年多期間，感謝梁勝富老師對我的研究教學和經驗傳承，使得我在面對許多事情時能更加得心應手，亦感謝蕭富仁老師從神經科學角度來指正研究，有了他們的指導，無論是研究上的疑難解答、研究方法、寫作方式、經驗分享等惠我良多，亦非常感謝腦科學研究中心所有全體成員，沒有大家的協助配合，許多事情就無法順利完成。

最後，我要感謝我的妻子培真在我求學期間對我的照顧和忍讓，替我分擔許多研究上的壓力與挫折，經常早出晚歸的我，常忽略了她孤獨的感受；在此亦感謝我的父母過去對我的栽培和鼓勵，教導我做人品德為最，強調人格健全之發展與學習生活之態度，由於他們辛勞的付出和細心的照顧，才有今天的我。謹以本文獻給我親愛的家人與親友們，以及關心我的師長，願你們共享這份榮耀與喜悅。

柯立偉　敬上

2007/10/11

Contents

List of Tables

List of Figures

1. Introduction

1.1 Motivation

Drivers' fatigue has been implicated as a causal factor in many accidents. Preventing accidents caused by drowsiness has become a major focus of active safety driving in recent years. During the past years, driving safely has received increasing attention of the publics due to the growing number of traffic accidents because of the marked decline in the drivers' abilities of perception, recognition and vehicle control abilities while sleepy. Therefore, it requires an optimal human estimation system to online continuously detect drivers' cognitive state related to abilities in perception, recognition, and vehicle control. The difficulties in developing such a system are lack of significant index for detecting drowsiness and complicated noise interferences in a realistic and dynamic driving environment. Development of the drowsiness monitoring technology for preventing accidents behind the steering wheel has become a major interest in the field of safety driving. Thus, developing accurate and non-invasive real-time driver drowsiness monitoring system would be highly desirable, particularly if this system can be further integrated into an automatic warning system.

It is known that abundant information on physiological changes such as eye activity measures, heart rate variability (HRV), or particularly, the electroencephalogram (EEG) activities can relate with drowsiness (Vuckovic et al., 2002; Roberts et al., 2000). Previous studies (Stern et al., 1994; McGregor and Stern, 1996) showed that the eye blink duration and the blink rate typically increases while blink amplitude decreases as function of the cumulative time, and the saccade frequencies and velocities of electrooculogram (EOG) decline when people get drowsy. Although approaches based on EOG signals showed that eye-activity

variations were highly correlated with the human fatigue and can accurately and quantitatively estimate alertness levels, the step size (temporal resolution) of those eye-activity based methods is relatively long (about 10 seconds) to track slow changes in vigilance (Orden et al., 2000). Contrarily, the step size of the EEG-based methods can be reduced to about 2 seconds to track second-to-second fluctuations in the subject's performance (Orden et al., 2001; Jung et al., 1997; Makeig and Jung, 1996). Since the computer power becomes faster and faster, it is practicable and appealing to know what information about human cognitive state and behavior are available through analyzing complex EEG signals. Hence, we constructed a virtual-reality (VR) based highway-driving environment to study drivers' cognitive changes during a long-term driving. A lane-keeping driving experiment was designed to indirectly quantify the driver's drowsiness level and a drowsiness estimation system combining the EEG power spectrum analysis, the principle component analysis (PCA) and the linear regression model was developed. Independent Component Analysis (ICA) was used in the similar experiments (Comon, 1994; Girolami, 1998; Lee et al., 1999) to locate the optimal electrode placements for each individual. A total of 10 frequency bands in 2 ICA components are selected and fed to the linear regression models to estimate driver's performance.

1.2 Statement of the Problem

Biomedical signal monitoring systems have been rapidly advanced with electronic and information technologies in recent years. Electroencephalogram (EEG) recordings are usually obtained by placing electrodes on the scalp with a conductive gel or paste, each of which is attached to a wire that is then connected to an external signal acquisition device. The tethering caused by this method of recording prohibits experiments in real operational environments. Furthermore, most of the existing

physiological signal monitoring systems can only record the signals without the capability of automatic analysis. In this study, we develop a portable and real-time Brain Computer Interface (BCI) that can acquire and analyze EEG signals in real-time to monitor human physiological as well as cognitive states and, in turn, provide warning signals to the users when needed. In order to widely application in the realistic environment, we should consider the effects of kinesthetic perception on the BCI system. Therefore, we first constructed the unique virtual reality-based dynamic driving environment to investigate EEG activation on kinesthetic perception and under different cognitive states. Then, the neural human machine interface/interaction in realistic environment will be well-established by combining the findings of EEG activation with the portable and real-time BCI system.

Kinesthetic perception is one of the most important sensations to human beings. The vestibular system thus plays an important role in our lives. We usually overlook the contributions of the vestibular system to our lives, simply because it doesn't give us the sense of this vivid and harmonic world the way our eyes and ears do. However, we would not have a complete sensation without the perception of motion. Vestibular system is one of the most important sensory apparatus for detecting the perception of motion. One of the most experienced kinesthetic perceptions in our life is the motion associated with driving. Almost all of the existing EEG correlated research studies of perceiving kinesthetic stimuli focus on the brain dynamics of the subjects receiving visual and/or auditory stimulus, very few one focus on the subject perception of kinesthetic stimulus such as car drivers, airplane pilots, etc.

After the investigation of kinesthetic perception, we would use the portable real-time BCI system as the base platform and increase some actual functions such as low-power consumption for portability and high computational capability to process EEG signal. The portable and real-time BCI system consists of a 4-channel bio-signal

acquisition/amplification module, a wireless transmission module, a dual-core signal processing unit and a host system for display and storage. The embedded dual-core processing system with multi-task scheduling capability was proposed to acquire and process the input EEG signals in real-time. In addition, the wireless transmission module, which eliminates the inconvenience of wiring, can be switched between radio frequency (RF) and Bluetooth according to the transmission distance. Finally, the real-time EEG-based drowsiness monitoring and warning algorithms were implemented and integrated into the system to close the loop of the BCI system. The practical online testing demonstrates the feasibility of using the proposed system with the ability of real-time processing, automatic analysis and on-line warning feedback in real-world operation and living environments.

Based on the neural human machine interface/interaction in the future work, we will perform more realistic experiments on the unique VR-based dynamic driving environment which can simulate vehicle driving and 3D surrounded scenes to investigate the EEG correlated activities of the driver (such as, distraction, carsickness (motion sickness), etc.). It will widen the fundamental biomedical and brain science research and spawns new industry opportunities to provide the solutions of real-life problems.

1.3 Organization of Dissertation

This dissertation is organized as follows. Chapter 2 describes the virtual reality-based dynamic driving environment, electroencephalogram (EEG) signal acquisition system, Independent Component Analysis (ICA), event-related potential (ERP), and event-related spectral perturbation (ERSP). Chapter 3 explores EEG activation of kinesthetic perception under our unique virtual-reality-based dynamic driving environment. Chapter 4 investigates EEG activation under different cognitive

states and develops drowsiness estimation technology by using Micro Electro Mechanical Systems sensor (MEMS sensor). Based on the drowsiness estimation technology, Chapter 5 develops the portable brain computer interface to real-time detect drivers' drowsiness. At last, we make some conclusions in Chapter 6.

2. Materials and Methods

2.1 Virtual-Reality-based Dynamic Driving Environment

In this study, we developed a VR-based 3D high-fidelity interactive highway scene, which was composed of seven identical PCs, synchronized by LAN, running the same VR program. The synchronized scenes were projected from seven projectors to constitute a surrounding vision (as shown in Figure 2-1. (a)). At the center of the projected scenes, we mounted a real vehicle (without the unnecessary weight of an engine and other components) on the motion platform to provide motion sensations as would be experienced in real driving (as shown in Figure 2-1. (b)). The vestibular cues, or motion cues, were delivered by a motion platform controlled by six hydraulic linear actuators. This hexapod configuration is also known as a Stewart Platform (Stewart, 1965). During driving in the real world, either deceleration or acceleration would occur even on smooth road. The platform generated accelerations in vertical, lateral, and longitudinal directions of a vehicle as well as pitch, roll, and yaw angular accelerations. To simulate a deceleration in driving motion, for instance, the driver would feel a force pushing him/her against the seat belt, and the platform would simultaneously tilt forward to change the gravity direction to simulate the deceleration force. Similarly, the platform would tilt backward to simulate an acceleration force. This (or comparable) technique has been used widely in driving simulation studies (Reymond and Kemeny, 2000).

In the VR-based dynamic environment and its emulation software, WorldToolKit (WTK) library and application programmer's interface (API) (Cardoso and Souloumiac, 1993) were reported in our previous study (Lin et al., 2005 & 2006). The detailed development diagram of the VR-based scene is shown in Figure 2-2.

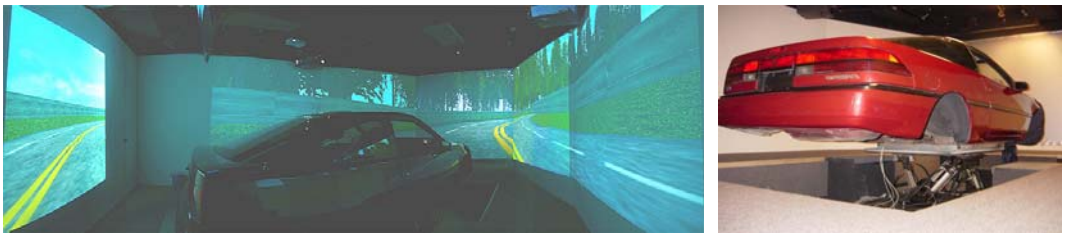

(a) (b)

Figure 2-1: (a) Kinesthetic virtual reality (VR) driving environment, (b) The driving cabin simulator mounted on a 6-DOF dynamic Stewart motion platform

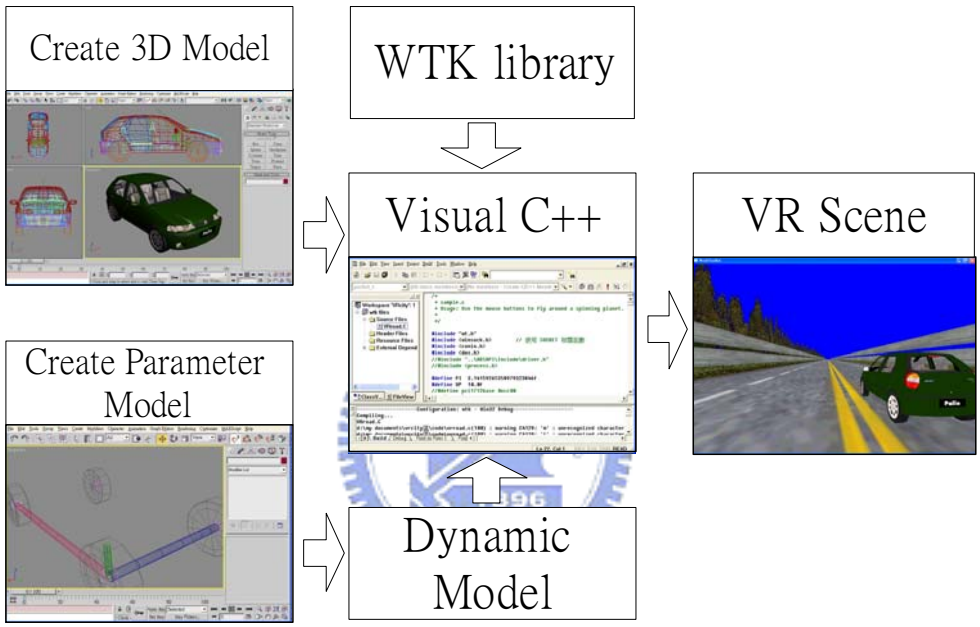

Figure 2-2: Flowchart of the VR-based highway scene developed environment. The dynamic models and shapes of the 3D objects in the VR scene are created and linked to the WTK library to form a complete interactive VR simulated scene

Firstly, we create models of various objects (such as cars, roads, trees and so on.) for the scene and set up the corresponding positions, attitudes, and other relative parameters. Then, we develop dynamic models among these virtual objects and build a complete simulated highway scene of full functionality with the aid of the high-level C-based API program. The VR-based four-lane highway scene is projected on a 120-surround screen (304.1-cm wide and 228.1-cm high), which is 350 cm away from

the driving cabin that is mounted on a 6-DOF Stewart motion platform. The four lanes from left to right are separated by a median stripe. The distance from the left side to the right side of the road is equally divided into 256 points (digitized into values 0-255, as shown in Figure 2-3), where the width of each lane and the car is 60 units and 32 units, respectively. These units can be converted to the real distance (for instance, the width of the real road is about 6 meters) in real-world applications. The refresh rate of highway scene is set properly to emulate a car driving at a fixed speed of 100 km/hr on the highway. The car is randomly drifted (triggered from the WTK program and the on-set time is recorded) away from the center of the cruising lane to mimic the consequences of a non-ideal road surface.

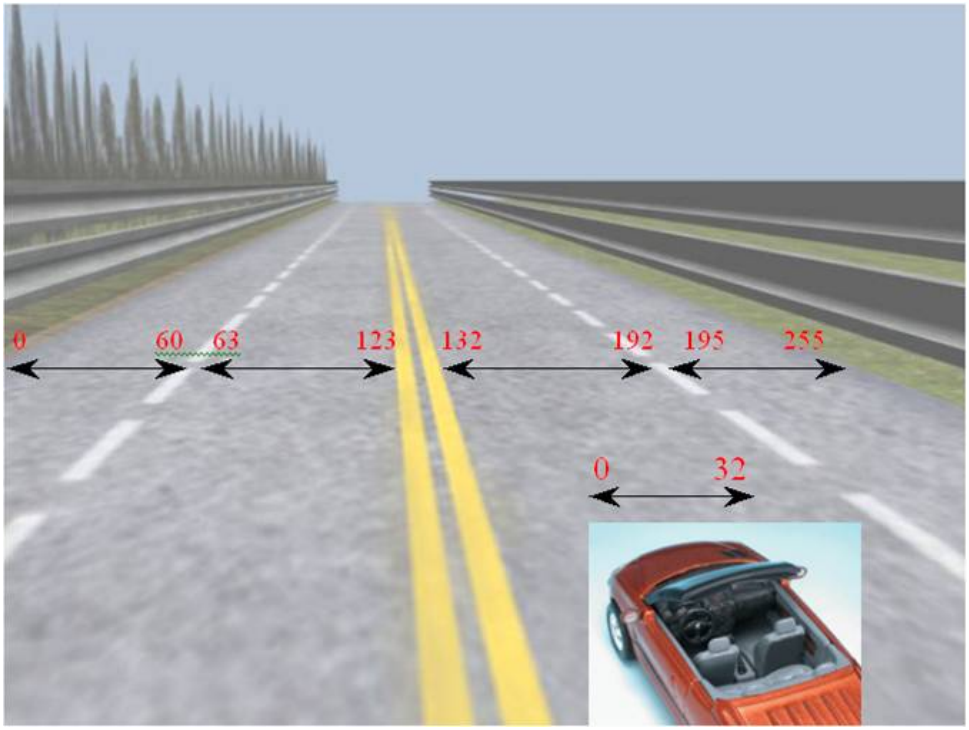

Figure 2-3: The width of highway is equally divided into 256 units and the width of the car is 32 units

To the best of our knowledge, the proposed environment setting is the first attempt at applying “kinesthetic” VR environment with motion platform techniques to

investigate brain activity in neuropsychological studies. The motion platform was conjugated with physiological and behavioral response recordings to offer more assessment options than the conventional neuropsychological studies could do. This was an innovative idea that provided an interactive, safe and realistic environment at very low cost. The VR technique allows subjects to interact directly with a virtual environment rather than passively responding to monotonic auditory and visual stimuli, and thus is an excellent setting for studying EEG dynamics in interactive and realistic tasks.

2.2 Electroencephalogram Signal Acquisition System

Subjects wore a movement-proof electrode cap with 36 sintered Ag/AgCl electrodes to measure the electrical activities of the brain. The physiological data acquisition used 2 bipolar ECG electrodes placed on the chest and 33 unipolar EEG/EOG electrodes placed based on a modified International 10-20 system (FP1/2, F3/4, F7/8, FZ, FC3/4, FT7/8, FCZ, C3/4, T3/4, CZ, CP3/4, TP7/8, CPZ, P3/4, T5/6, PZ, O1/2, OZ, VEOU, VEOL, A1) and refer to the mean of the left and right mastoid electrodes. Figure 2-4 shows the 32 channel EEG electrode cap. All EEG channels were located based on a modified International 10-20 system as shown in Figure 2-5 (Thakor, 1999). The 10-20 system is based on the relationship between the locations of an electrode and the underlying area of cerebral cortex.

Figure 2-4: The 32 channel EEG electrode cap

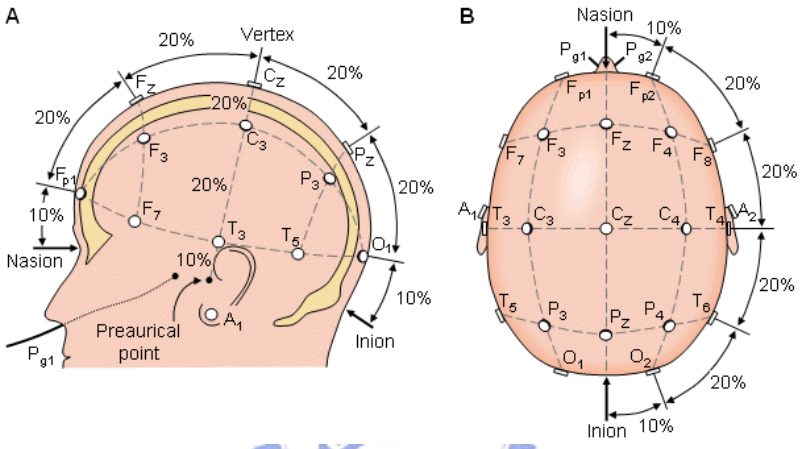

(a) The lateral view (b) The top view

Figure 2-5: The International 10-20 system of electrode placement

Before data acquisition, the contact impedance between EEG electrodes and scalp was calibrated to be less than 5kΩ by injecting NaCl-based conductive gel. We used the Scan NuAmps Express system (Compumedics Ltd., VIC, Australia), a high-quality 40-channel digital EEG amplifier capable of 32-bit precision sampled at 1000 Hz, to simultaneously record the EEG/EOG/ECG data and the deviation between the center of the vehicle and the center of the cruising lane triggered by the VR program. The EEG data were band-passed between 0.5 and 100Hz with a 60Hz notch filter, and recorded with 16-bit quantization level at a sampling rate of 500 Hz and then down-sampled to 250 Hz for the simplicity of data processing.

2.3 Independent Component Analysis

Independent Component Analysis (ICA) is a signal processing technique that finds a linear mapping matrix or unmixing matrix W such that the unknown unmixed signals of the dimension N, $U(t) = [u_1(t), \ldots, u_N(t)]^T$ could be separated from their mixtures, $X(t)$, that is $Y(t) = W^{-1}X(t)$. The ICA methods were extensively applied to blind source separation problem since 1990s (Jutten et al., 1991; Comon, 1994; Bell et al., 1995; Girolami, 1998, Lee et al., 1999). Subsequent technical reports (Jung et al., 1998, 2000, & 2001; Naganawa et al., 2005; Liao et al., 2005) demonstrated that ICA was a suitable solution to the problem of EEG source segregation, identification, and localization.

In this study, we used an extended version of informax algorithm of Bell and Sejnowski (1995) that can separate sources with either super- or sub-Gaussian distributions, to decompose distinct brain activities. After ICA training, we can obtain 33 ICA components decomposed from the measured 33-channel EEG data. It has also been used in our previous study (Lin et al., 2005). Figure 2-6 shows the scalp topographies of ICA back-projection matrix W^{-1} of one subject and the log bandpower spectra of all ICA components, which provide information about the location of the sources. For instance, eye activity was projected mainly to frontal sites. Hence, most of the eye-movement artifacts are isolated to components 1-3, as shown in Figure 2-6. The drowsiness-related potential is on the parietal lobe to occipital lobe. We can observe that the ICA components 8, 17, and 27 may be considered as effective "sources" related to drowsiness in the VR-based dynamic driving experiment (based on the correlation analysis in chapter 4).

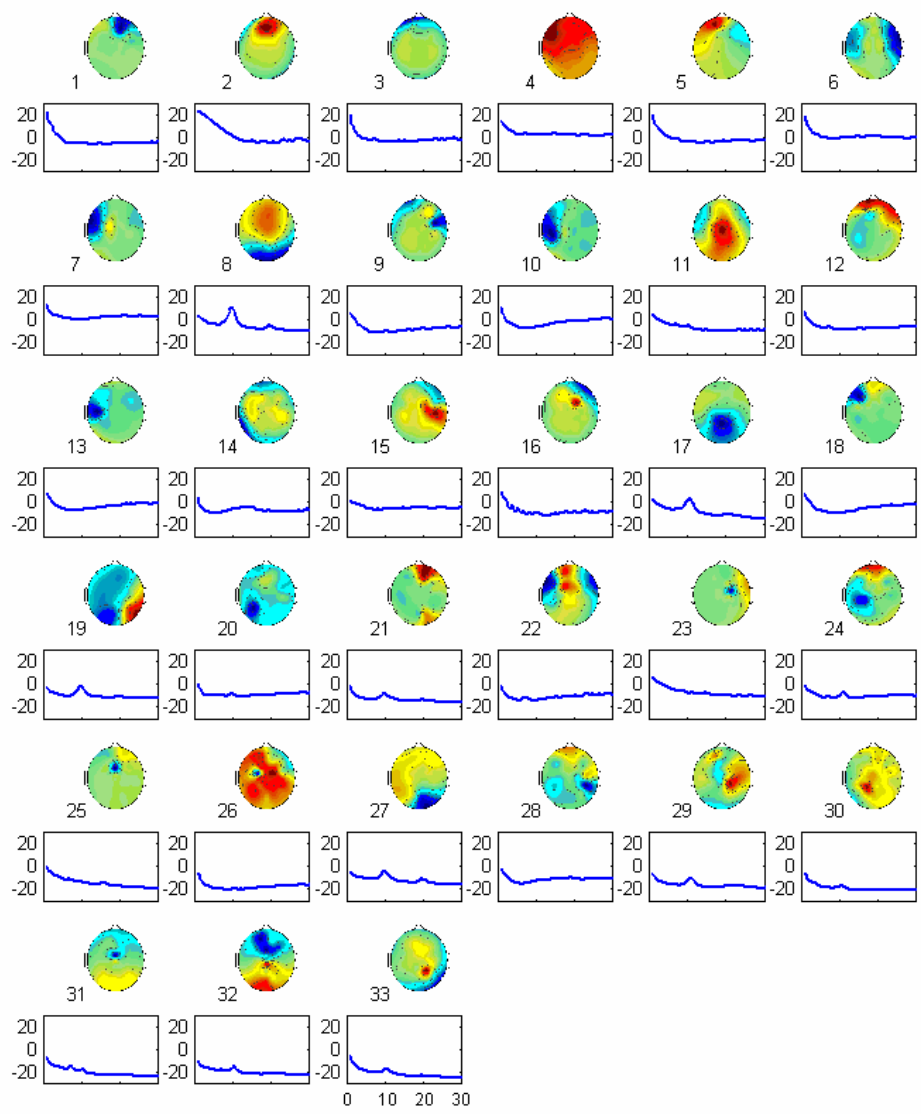

Figure 2-6: The scalp topographies and the corresponding log bandpower spectra of all ICA components.

2.4 Event-Related Potential

Single-trial event-related potential (ERP) data are usually averaged prior to analysis to increase their signal/noise relative to non-time and -phase locked EEG activity and non-neural artifacts. The ERP is much smaller than the amplitudes of ongoing EEG, and it is thus often buried in the EEG recordings. In order to extract the ERP from EEG signal, we need to increase the signal to noise ratio by presenting the same type of stimuli to the subject repeatedly. ERP is often obtained by averaging

EEG signals of accumulated single trails of the same condition. Ongoing EEG signals across signal trails are considered random and independent of the stimulus. However, it is assumed that the waveform and latency of ERP pattern are invariant to the same stimulus. Through phase cancellation, time- and phase-locked EEG signals will be more prominent.

Event-Related Potential (ERP) images directly visualized single event-related EEG trials and their contributions to the averaged ERP (Jung et al., 2001). An ERP image also makes visible relationships between subject behavior and amplitudes/latencies of individual event-related responses. The limitation of ERP is that it only measures coherent time-and-phase-locked activities. Averaging same response epochs would involve phase cancellation, brain activities not exactly synchronized in both time and phase are averaged out.

2.5 Event-Related Spectral Perturbation

The event-related spectral perturbation (ERSP) measures average dynamic changes in amplitudes of the broad band EEG spectrum as a function of time following cognitive events. The processing flow is shown in Figure 2-7. The time sequence of EEG channel data or ICA activations are subject to Fast Fourier Transform (FFT) with overlapped moving windows. Spectrums prior to event onsets are considered as baseline spectra. The mean baseline spectra were converted into dB power and subtracted from spectral power after stimulus onsets so that we can visualize spectral perturbation from the baseline. To reduce random error, spectrums in each epoch were smoothed by 3-windows moving-average. This procedure is applied to all the epochs, the results are then averaged to yield ERSP image. Through ERSP, we are able to observe time-locked but not necessarily phase-locked activities. ERSP thus can reveal aspects of event-related brain dynamics which might not be

measurable in ERP averages of the same response epochs (Makeig, 1993). In this study, we applied both ERP and ERSP analysis on the EEG data acquisition in our experiments.

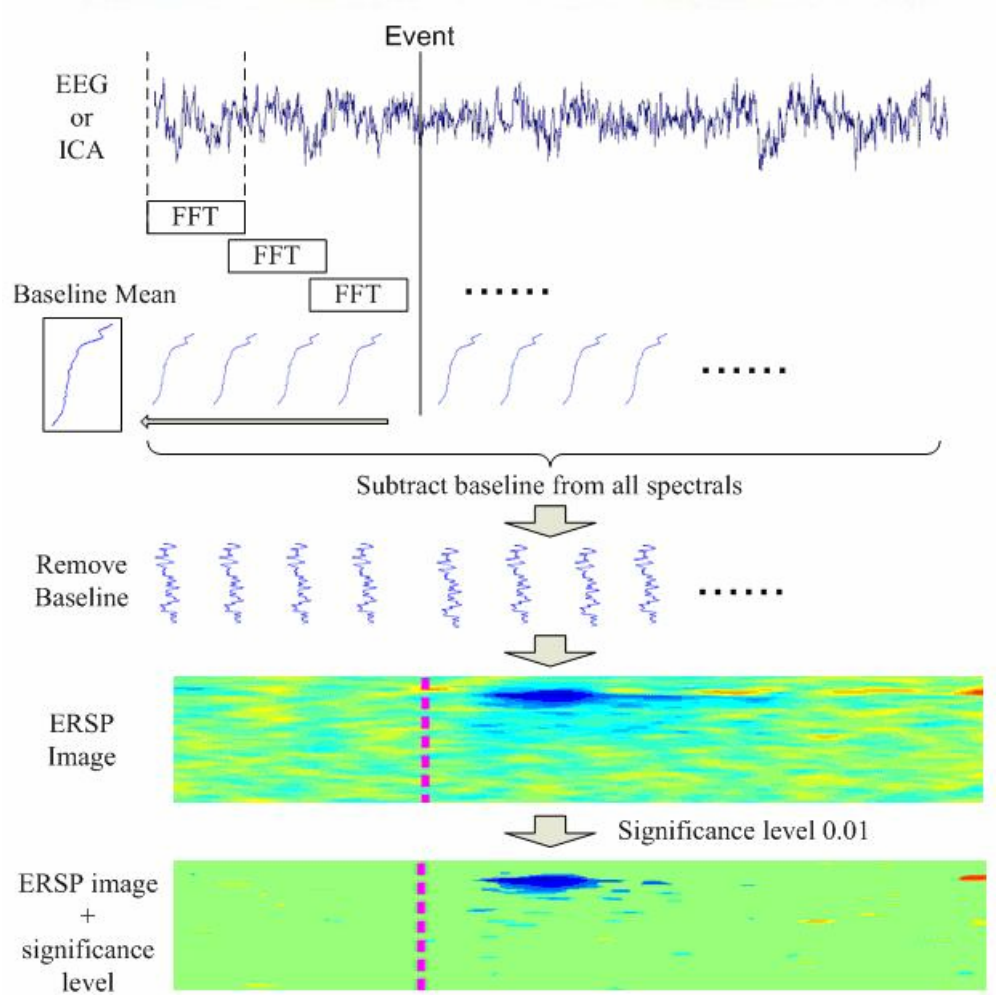

Figure 2-7: Event-related spectral perturbation plot. ERSP plots the grand mean time course of changes from pre-stimulus baseline in log spectral power of a scalp-recorded EEG or ICA component activation time-locked to stimulus presentation or subject responses across frequencies.

3. EEG Activation of Kinesthetic Perception

3.1 Introduction

Kinesthetic perception -- the sensory apparatus that detects motion -- is one of the most important sensations to human beings, yet we usually overlook the contributions of the vestibular system to our lives, simply because it doesn't give us the sense of this vivid and harmonic world the way our eyes and ears do. In addition, kinesthetic perception doesn't involve taste or smell, making it less appreciated. But, we would not have a complete sensation of the world without the perception of motion. Vestibular system is one of the most important sensory apparatus for detecting the perception of motion. One of the most common kinesthetic perceptions in our life is the motion associated with driving. Almost all of the existing EEG correlated research studies of perceiving kinesthetic stimuli focus on the brain dynamics of the subjects receiving visual and/or auditory stimulus, very few one focus on the subject perception of kinesthetic stimulus such as car drivers, airplane pilots, etc.

In this chapter, we investigated EEG dynamics in response to kinesthetic stimuli by using the dynamic VR driving environment. This dynamic VR environment mimicked visual-vestibular co-stimulation during driving. Using simple driving behaviors such as deceleration, acceleration, and deviation, we studied brain responses of kinesthetic inputs by comparing subjects' EEG differences in motion (while the motion platform is active) and motionless (while the motion platform is inactive) conditions of the dynamic platform.

3.1.1 Vestibular system and kinesthetic stimulus response

The human vestibular system is a sensory apparatus located bilaterally in the

inner ears which detects the motion of the head and body in space (Berthoz, 2000). It is composed of two functional parts: the otolithic organs and the semicircular canals. The otolithic organs detect linear accelerations, while the semicircular canals detect rotary accelerations (Merfeld et al., 1999; Seidmann et al., 1998). Vestibular information plays an important role in perceptual tasks such as ego-motion estimation (Berthoz et al., 1995). In recent research, vestibular information was shown to disambiguate the interpretation of dynamic visual information during an observer's movement (Wexler et al., 2001). Researchers have tried to measure evoked potentials of vestibular origin for 30 years. Elidan et al. (1991) reported the ERP response to high speed and transient vertical Z axis rotation. Subjects were rotated at the speed of 10,000°/sec2 for 2 ms. The reported negativity peaked at about 15 ms after the onsets of rotation from signals measured at a forehead mastoid electrode. Baudonniere et al. (1999) reported a biphasic negative wave, that is most prominent at central midline electrode (Cz) in subjects who received short (30 ms) linear displacements without co-stimulation of the semicircular canals.

Probst et al. (1993, 1996, & 1997) and Loose et al. (2002) observed bell-shaped negativity at central midline channels following roll up and down motion along the X axis. The Vestibular Evoked Potential (VESTEP) evoked by stimulating otolithic and semicircular canals with different orientations of rotations or directions of movements was investigated in depth. The experimental variables in these studies were well controlled; for instance, subjects were blindfolded in VESTEP investigations, or watched pixels moving or rotating on the screen. This might be desirable from the perspective of scientific research, but is less practical because we rarely experience vestibular stimulation without visual co-stimulation or watch pixels rotating or moving in the real world. We actually live in a visual-vestibular co-stimulation world and the visual cue is always a meaningful and continuous scene

-- in driving, for instance.

3.1.2 Kinesthetic perception during driving

One of the most experienced kinesthetic perceptions in our life is the motion associated with driving. Whenever our vehicle accelerates, decelerates, or curves around a corner, we experience a force pulling our body against the direction of motion. However, there are at least several major obstacles in investigating the driving perception in a real driving environment. First, the safety concerns dictate that experiments must be conducted in a safe driving environment, making it an ethic issue to conduct driving experiments on the road while experiments know the subject might experience attentions lapse during experiments. Second, appropriate data acquisition and monitoring are needed for studying the rapid physiological responses of kinesthetic stimuli. The stimulation should be simple enough and repeatable to keep the experiment under control. Last, objective evaluation should be assessed in the studies. A driver senses not only the pushing or pulling force, but also the scene changes related to the movement of the vehicle. The driving perception includes the co-stimulation of visual cue, vestibular stimulation, muscle reaction, and skin pressure.

This is indeed a complicated mechanism to understand. One of our solutions is to conduct driving experiments using a realistic simulator, which is widely used in driving-related research (Kemeny et al., 2003). Regarding the necessity of motion during driving, the literature shows that the absence of motion information increases reaction times to external movement perturbations and decreases safety margins in the control of lateral acceleration in curve driving (Reymond et al., 2001). In real driving, improper signals from disordered vestibular organs were reported to contribute to inappropriate steering adjustment (Page and Gresty, 1985). Groen et al. (1999) also

showed that the presence of vestibular information in driving simulators was important in the perception of illusory self-tilt and illusory self-motion. These studies emphasized the importance of motion perception during driving to the assessment of driving performance and behavior. However, assessing driving performance or behavior is not objective enough since the performance and behavior varies due to the subject's training or learning effect. In this paper, we use a direct and objective method to evaluate human cognition during driving.

3.1.3 EEG studies under VR based dynamic driving

The EEG is a complex signal, the statistical properties of which depend on both time and space. Regarding the temporal characteristics, it is essential to note that EEG signals are ever-changing. The EEG has been used for 80 years in clinical practice as well as basic scientific studies. It is a popular method for evaluating human cognition today, which directly measures brain responses to external or internal stimulation. Much more information can be obtained from an EEG than from appearance behavior. Compared to another widely used neuro-imaging modality, functional Magnetic Resonance Imaging (fMRI), the greatest advantage of EEG is speed-it can record complex patterns of neural activity occurring within fractions of a second after a stimulus has been presented. EEG acquisition is also much less expensive, more portable and the only modality in which subjects allow to move their heads, thus it is applicable in operational environments such as driving in the moving vehicle.

In recent years, researchers have designed the Virtual Reality (VR) senses to provide appropriate environments for assessing brain activity during driving (Lin et al., 2005; Eoh et al., 2005). Lin et al. (2005) introduced the "dynamic" VR environment, that is, a VR scene with a motion platform, in conjunction with physiological and behavioral response recordings to offer more assessment options

than were available in traditional neuropsychological studies. This was an innovative idea that provided an interactive and realistic environment at very low cost and avoided the risks of operating an actual vehicle on the road. However, the EEG correlates of kinesthetic stimulations induced by the motion platform in the dynamic VR scene have not been fully assessed or appreciated.

To solve the aforementioned problems in studying kinesthetic perceptions during driving, using the realistic simulator is a good alternative used in driving-related research (Page and Gresty, 1985; Reymond et al., 2001; Groen et al., 1999; Eoh et al., 2005). Those studies primarily emphasized on the importance of motion perception during driving by assessing subjects' driving performances and behaviors. But such evaluations may be not objective enough since the performances and behaviors could vary with the subject's previous training or learning experiences. To simulate the more realistic driving condition, we have designed an interactive Virtual Reality (VR) scenes and a dynamic driving simulator to provide appropriate environments for assessing brain activity during kinesthetic driving (Lin et al. 2005). The "kinesthetic" VR environment is a VR scene with a motion platform controlled by the six hydraulic linear actuators. During the driving experiment, all scenes are continuously updated according to the displacement of the car and the subject's wheel handling.

3.2 Experiment Setup

3.2.1 Driving Events

We designed three driving events: stop, go, and deviation in the development virtual reality-based dynamic driving environment. The stop and go events were paired into a Stop-Go event, which means a stop event was always followed by a go event. The deceleration and acceleration in a Stop-Go event was controlled by a computer program. Figure 3-1 shows the time course of a typical Stop-Go event.

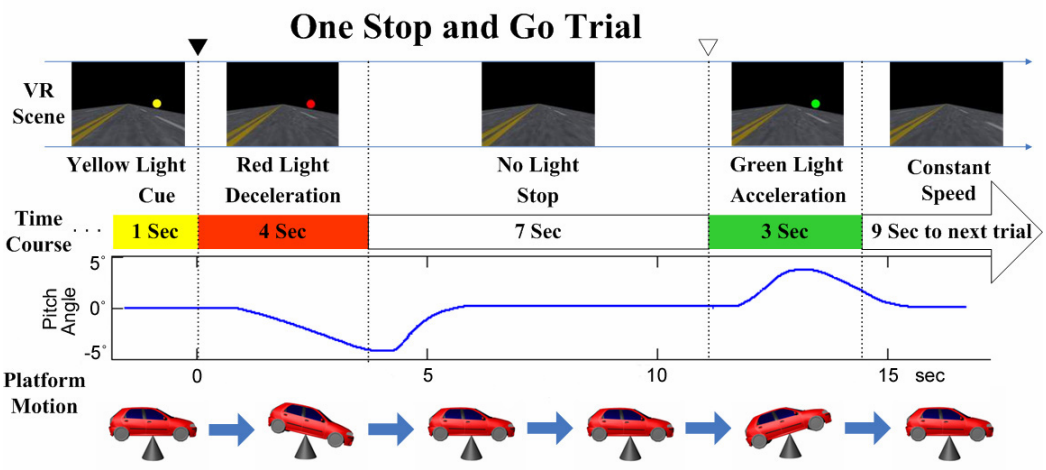

Figure 3-1: Illustration of the design for Stop-Go events in driving. The time course is cut into five sections. The top-panel pictures show the VR scenes in the sections, the blue trace shows the pitch angle of the hexapod motion platform, and the bottom panels depict the posture of the vehicle mounted on the motion platform. An event starts with a yellow-light cue displayed on the screen. One second later, the yellow light is replaced by a red light and a Stop-Go event begins in conjunction with a deceleration simulated by the motion platform. The car is slowed down to a complete stop in four seconds when the red light is out. Seven seconds later, a green light is shown on the screen, and a go event begins. The hexapod motion platform starts accelerating for 3 seconds. Then the green light goes off, and the vehicle is moving at a constant speed until the next event occurs.

Subjects were not required to take any action in the stop and go events during the experiment so that it can avoid the artifacts caused by the movement of the subjects. Moreover, the vehicle was randomly drifted away from the cruising position, which was defined as a deviation, and the subjects were instructed to steer the vehicle back to the center of the cruising lane as quickly as possible. The deviation events can keep subjects' attention and we can estimate the subjects' cognitive level from the reaction times. The driving behavioral information, such as the onsets of the deviation, subject reaction times, or steering angles, were recorded for further analysis.

Figure 3-2 illustrates a deviation event in which the vehicle was moving forward in a straight line. The vehicle deviated either to the left or to the right. The Stop-Go event and deviation event occurred randomly with the probability of 50% and the inter-event interval was 9 seconds.

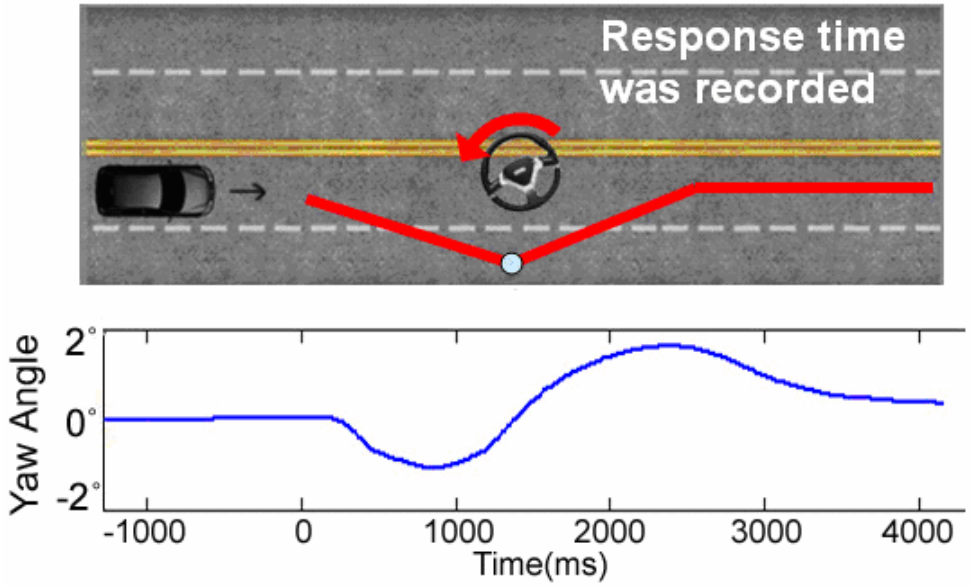

Figure 3-2: The vehicle was randomly drifted away from the cruising position, which was defined as a deviation event, and the subjects were instructed to steer the vehicle back to the center of the cruising lane as quickly as possible. The driving behavioral information, such as the onsets of the deviation, subject reaction times, or steering angles, were recorded for further analysis. In a deviation event, the vehicle was moving forward in a straight line. The vehicle deviated either to the left or to the right. The Stop-Go event and deviation event occurred randomly with the probability of 50% and the inter-event intervals were 9 seconds.

3.2.2 Subjects and EEG Data Acquisition

Ten right-handed, healthy subjects (aged between 20 and 28) participated in this study. All subjects had driving license and at least one-year driving experience. Subjects were instructed to keep the car at the center of the inside lane by controlling

the steering wheel, and to perform the driving task consciously. Each subject completed four 25-minute sessions of the driving experiment. Sessions were motion and motionless counterbalanced and each session included stop-go events and deviation events in random order. Thus we have six conditions: “Motion-Stop,” “Motion-Go,” “Motion-Deviation,” “Motionless-Stop,” “Motionless-Go,” and “Motionless-Deviation.” To prevent subjects from experiencing drowsiness during experiments, they rested for a few minutes after each session until they were ready for the next one. The entire driving experiment lasted about 2 hours. Subjects performed at least 2 driving experiments on different days for testing the cross-session consistency.

Subjects wore the movement-proof electrode cap with 36 sintered Ag/AgCl electrodes to simultaneously record the EEG/EOG/ECG data and the deviation between the center of the vehicle and the center of the cruising lane triggered by the VR program. In addition, an accelerometer recording 3-DOF (Degrees of Freedom) was placed on the center of the vehicle to record the platform movement. This accelerometer recorded orientations of the vehicle in pitch, roll, and yaw during the driving simulation, thus we could correlate physiological data with the orientation recording and investigate the relationship between human cognition and kinesthetic stimulus.

3.2.3 EEG Data Analysis

The recordings were down-sampled to 250 Hz for simplicity of data processing. Then the EEG data were preprocessed using a simple low-pass filter with a cut-off frequency of 50 Hz to remove the line noise (60 Hz and its harmonic) and other high-frequency noises for further analysis. The continuous EEG signals were first extracted into epochs whose lengths were designed to cover the whole platform

dynamics in single driving events. For stop events and go events, epochs contained EEG data from 4s before to 9s after the onsets of the red light. For deviation events, epochs contained signals from 1s before to 2s after the deviation onsets. We then applied ICA to concatenated epochs to decompose them into temporally statistical component activations.

To study the cross-subject component stability of ICA decomposition, components from multiple sessions and subjects were clustered based on their spatial distributions and EEG characteristics (Jung et al., 2001; Makeig et al., 2004).

Component clustering grouped massive components from multiple sessions and subjects into several significant clusters. Cluster analysis, k-means, was applied to the normalized scalp topographies and power spectra of all 930 (30 channels x 31 sessions) components from the 10 subjects. After ICA decomposition, noisy components were removed prior to cluster analysis. The cluster analysis, k-means, identified at least 9 clusters of components having similar power spectra and scalp projections. These component clusters also showed functionally distinct activity patterns. Nine distinct component clusters (as shown in Figure 3-3) accounted for eye blinks (upper left), horizontal eye movements (upper right), and other brain activities, respectively. Artifactual components accounted for such as eye blinks and horizontal eye movements were effectively removed from the activity of the other seven component clusters by the ICA decomposition and are not further considered here.

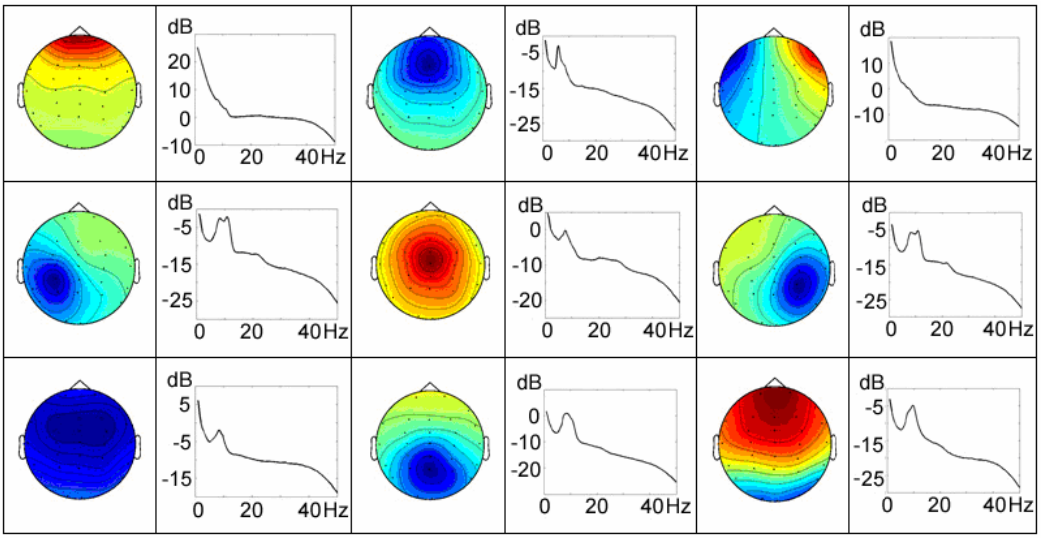

Figure 3-3: The ICA components from 11 subjects are clustered into 9 groups. The averaged scalp map and averaged baseline (before event onsets) power spectral density of each group are shown in the plot. The motion-related features are found in left-mu (middle-left), right-mu (middle-right), and central-midline (middle) components.

3.3 Experiment Results

The sessions in each experiment were divided into “motion” (when the motion platform was in action) and “motionless” (when the motion platform was not in action) sessions with stop, go, and deviation events. According to the behavioral data of the deviation events, all subjects’ response time are less than one second (as shown in Table 3-1). This indicated that all subjects were alert and attentive during the whole sessions. We get six conditions: “Motion-Stop,” “Motion-Go,” “Motion-Deviation,” “Motionless-Stop,” “Motionless-Go,” and “Motionless-Deviation” after the subjects have performed all the experiments. By comparing the motion and motionless pair, we hope to find some differences in brain responses between these two conditions.

Table 3-1: The response time (RT) of Motion-Deviation and Motionless-Deviation events. Overall, the RT in dynamic driving is 40~50 ms shorter than that in static driving. These results were obtained using PRISM.

		Mean	N	Std. Deviation	Std. Error Mean
Pair 1 Dev. Left	Motion V1	754.097	846	269.6578	9.2710
	Motionless V3	812.566	846	251.1152	8.6335
Pair 2 Dev. Right	Motion V2	730.491	827	295.6911	10.2822
	Motionless V4	769.549	827	291.2164	10.1266

3.3.1 Effects of Kinesthetic Stimuli in Mu Component Activations

Figure 3-4 shows the ERSP of a component from a typical subject that exhibited differential brain responses between motion and motionless conditions. The component scalp map exhibited the defining features of mu rhythms -- distinct spectral peaks near 10 Hz and 22 Hz, with equivalent dipoles located roughly over hand motor cortex (and/or adjacent post-central somatosensory areas), and oriented roughly orthogonal to the directions of the central sulci. The upper ERSP panels show the ERSP following stop events, while the lower two show go-event ERSP. Images on the left are brain responses under “motion” conditions and those on the right are under “motionless” conditions. The curves below the images are the time courses of the platform motion (pitching, rotate by Y axis). Mu power was strongly blocked (reduced) around the peak of platform motion in Motion-Stop and Motion-Go events. In contrast, no mu blocking occurred following either stop or go events in the motionless condition (Figure 3-4, right panels). Thus the mu blocking appears to be induced by the kinesthetic inputs in stop and go events.

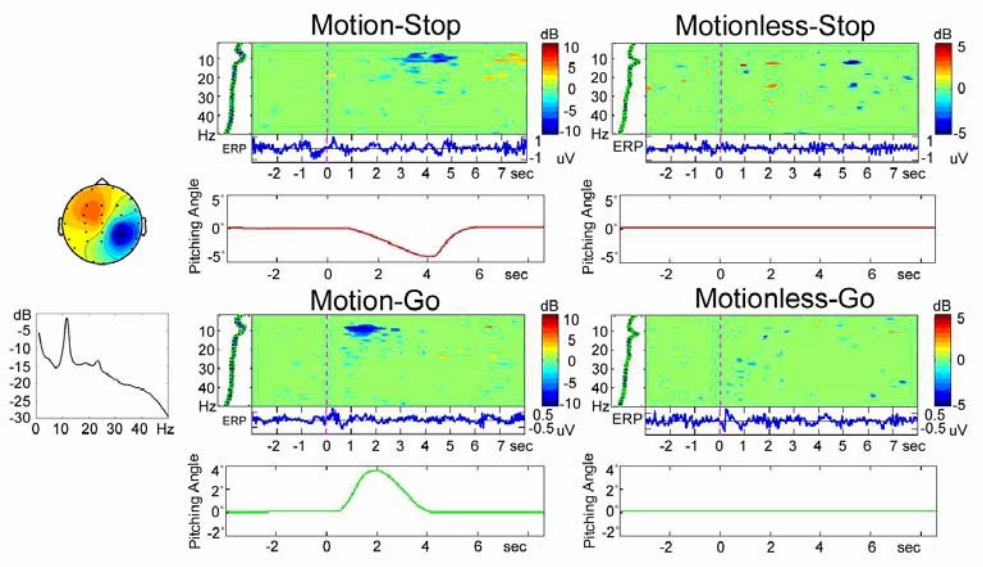

Figure 3-4: A right mu component shows mu characteristic 10 Hz and 22 Hz peaks in the activity spectrum (lower left). The component mean ERSP shows mean event-related changes in (log) spectral power across data trials time-locked to the kinesthetic stimulus onsets (dashed line). Following the motion platform movement, this activity is blocked. The activity was unchanged from the baseline spectra if the motion platform was not in action (right).

Mu blocking was also observed following deviation events. Figure 3-5 shows the ERSP of a right mu component following deviation events. The upper and lower panels show ERSPs of the component following "deviate-to-left" and "deviate-to-right" events, respectively. The curves below show the recorded platform motion. Notice that the motion platform tilted along different directions in Stop-Go and deviation events (cf. Figure 3-5). In deviation events, the platform rotated slightly along the vertical Z axis.

When deviation occurred, the subjects were instructed to maneuver the car back to the cruising position by steering the wheel. It is expected that mu activity would be blocked due to the hand movement (cf. Figure 3-5 ERSP) in both motion and motionless conditions. However, the latency of mu blocking in the motion condition

(Figure 3-5 left panels) was significantly shorter than that in the motionless condition (Figure 3-5 right panels).

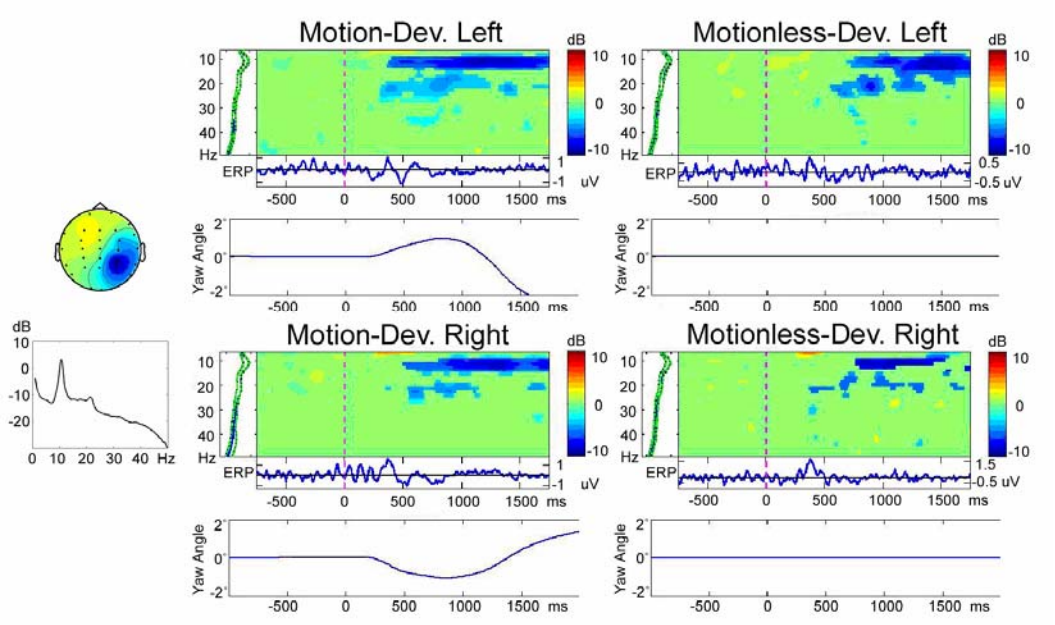

Figure 3-5: The mean ERSP of the mu component following deviation events. The upper panels correspond to deviate-to-left events, and the lower panels correspond to deviate-to-right events. The left panels show the ERSP of the component when the motion platform was in action (Motion-Deviation), while the right panels plot the ERSP when the platform was not in action (Motionless-Deviation). Mu blocking appears in all four conditions, but the latencies of the activation were shorter in Motion-Deviation (left panels) than those in motionless conditions.

3.3.2 Effects of Kinesthetic Stimuli in Central Midline Component Activations

Figure 3-6 shows the scalp map and dynamic properties of an independent component from the same subject in Motion-Deviation and Motionless-Deviation conditions. The scalp map of the CM component (Figure 3-6 upper left) resembles scalp maps of the “P3a” or “P3novel” ERP peaks seen, for example, when unique and unexpected stimuli are included in a randomly alternating sequence of target and

non-target stimuli (Polich and Comerchero, 2003). In two-dimensional "ERP image" plots of single trials from the subject, potential fluctuations in single trials are shown as color-coded horizontal lines, here normalized by component activation baseline variability then sorted (across all trials) by response time (RT). The ERP images clearly show that the early kinesthetic response, peaked at ~250 ms, was time-locked to deviation onset. However, this sharp negativity was missing in the motionless condition (Figure 3-6 right panels). We suspect that the negativity was primarily induced by the platform motion.

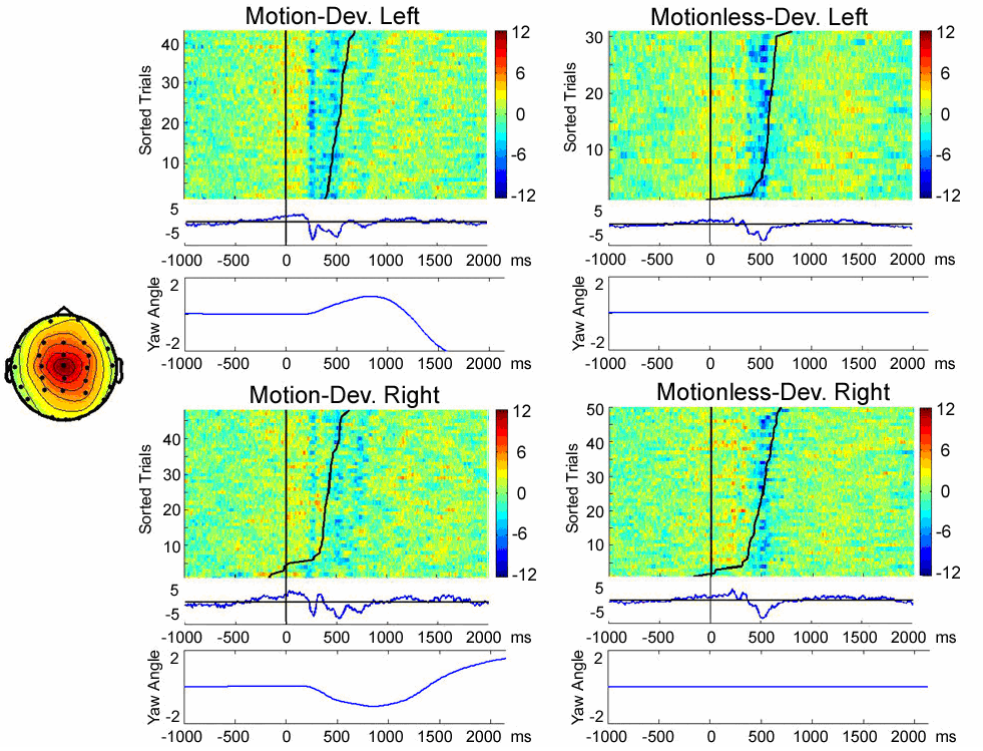

Figure 3-6: Single-trial Event-Related Potentials (ERPs) of the central midline (CM) component following deviation events under 4 different conditions. The upper two panels plot ERSP in deviate-to-left events, and the lower two panels plot ERSP in deviate-to-right events. The left panels correspond to Motion-Deviation, while the right panels correspond to Motionless-Deviation. The averaged ERPs exhibit a strong negative peak 500 ms after deviation onsets in all 4 conditions, however the negativity peaks ~250 ms post-event are only evoked by the deviation events when the platform

is in action (Motion-Deviation).

3.3.3 Effects of Kinesthetic Stimuli in Component Clustering Results

Figure 3-7 shows the mean map and power spectrum of a large cluster of left mu components. The power spectra of the component cluster contained peaks near 11 and 20 Hz. In all 29 components from 10 subjects contributing to this cluster, the 11 Hz activity was blocked following kinesthetic stimuli in the motion condition, strongly suggesting that these represented mu activity. Scalp maps of individual left mu components in this cluster (Figure 3-7 right panels) strongly resembled the (left) cluster mean map.

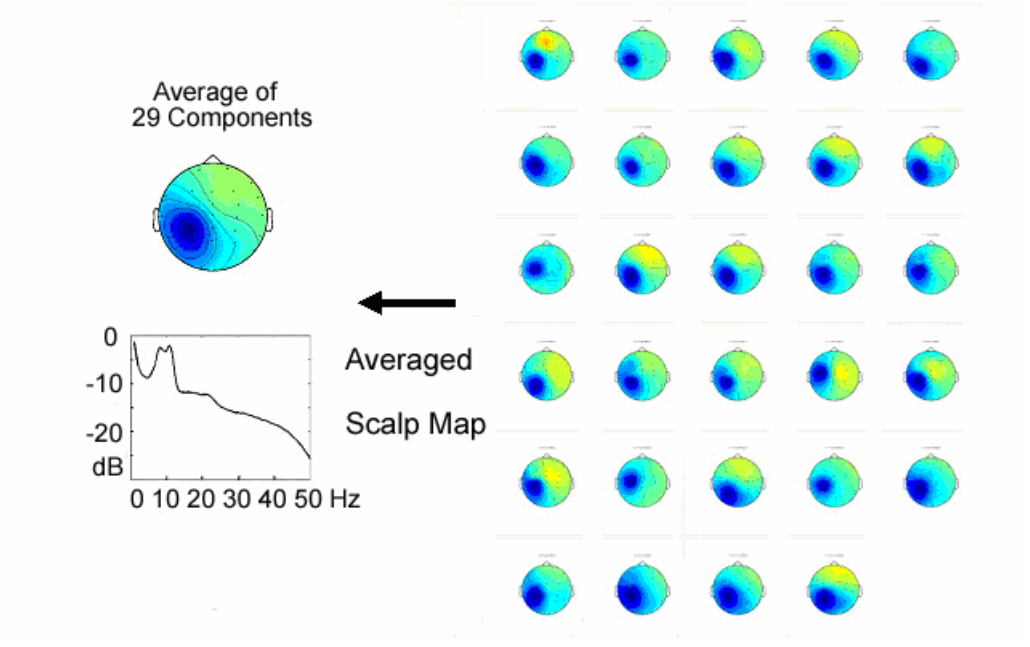

Figure 3-7: Mean (N=29) component map and mean power spectra of a left-mu component cluster. Individual component maps resembled the averaged scalp map.

Figure 3-8 shows the component cluster mean ERSP of the component activations following Stop-Go events under the motion (left panels) and motionless (right panels) conditions. The ERSP images of motion sessions exhibited a strong mu

blocking and alpha rebound, which were completely missing from the ERSP images under motionless conditions, consistent with the results in a typical subject shown in Figure 3-4.

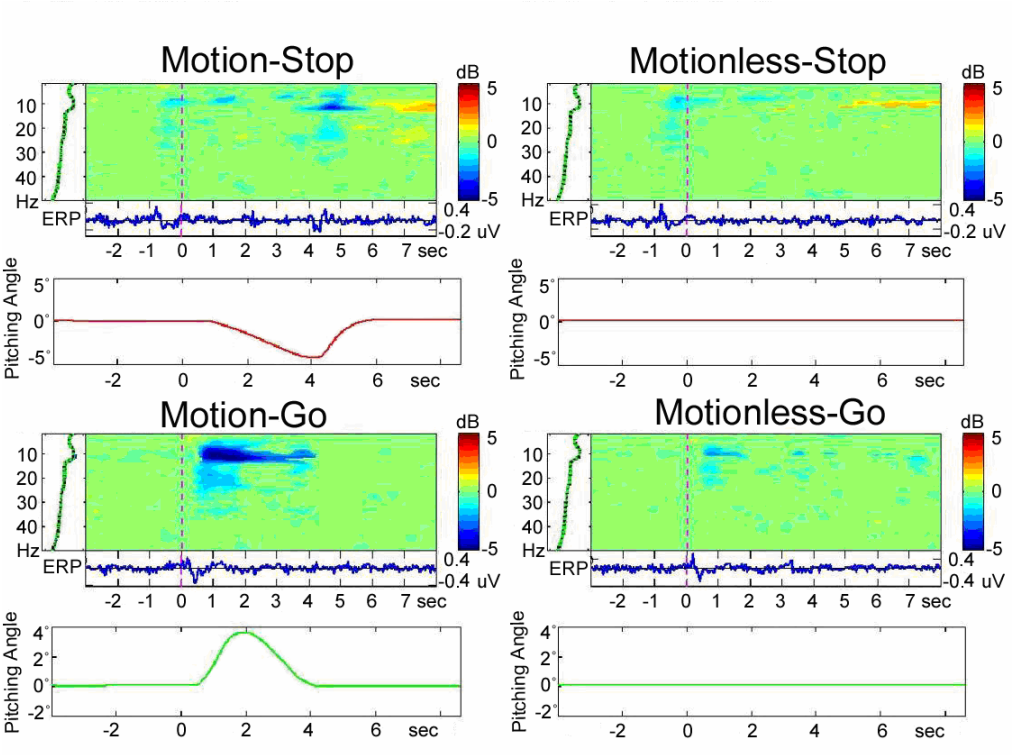

Figure 3-8: The group-averaged ERSP shows the component activations following Stop-Go events under the motion (left panels) and motionless (right panels) conditions. The ERSP images of motion sessions exhibited a strong mu blocking and alpha rebound, which were completely missing from the ERSP images under motionless conditions, consistent with the results in a typical experiment shown in Figure 3-4.

Similarly, Figure 3-9 shows averaged ERSP images following deviation events under motion and motionless conditions. Although the ERSP images in all four conditions exhibited similar mu blocking induced by the steering actions, the latencies of mu blocking differed considerably. Figure 3-10 shows the differences between mu blocking in motion and motionless conditions, which were obtained by subtracting the

motionless ERSP (right panels of Figure 3-9) from the motion ERSP (left panels of Figure 3-9). The dashed line marks average response time. A brief (~200 ms) alpha-band power suppression was evident in these two ERSP difference images, indicating that the mu blocking occurred earlier in Motion-Deviation events than in Motionless-Deviation events. No significant differences were found in the rest of the ERSP difference images. The subtracted images showed that mu blocking occurred 200 ms earlier in Motion-Deviation.

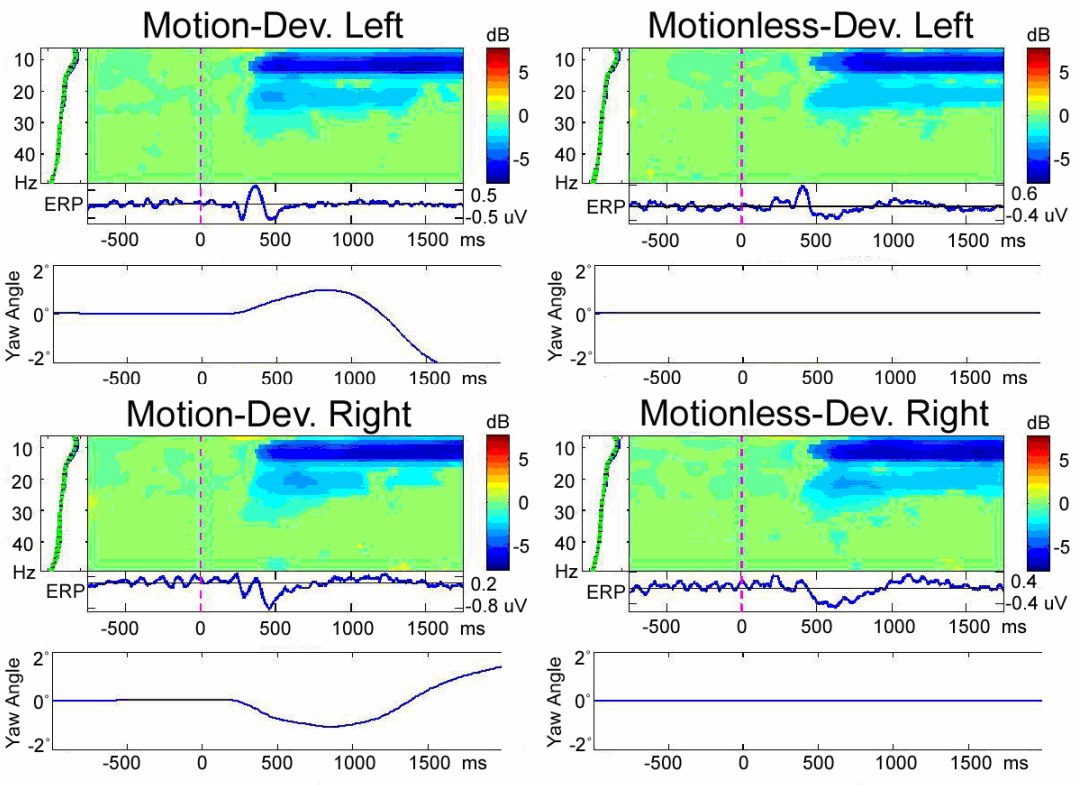

Figure 3-9: The group-averaged ERSP images following deviation events under motion and motionless conditions. Although the ERSP images in all four conditions exhibited similar mu blocking, the latencies of mu blocking differed considerably.

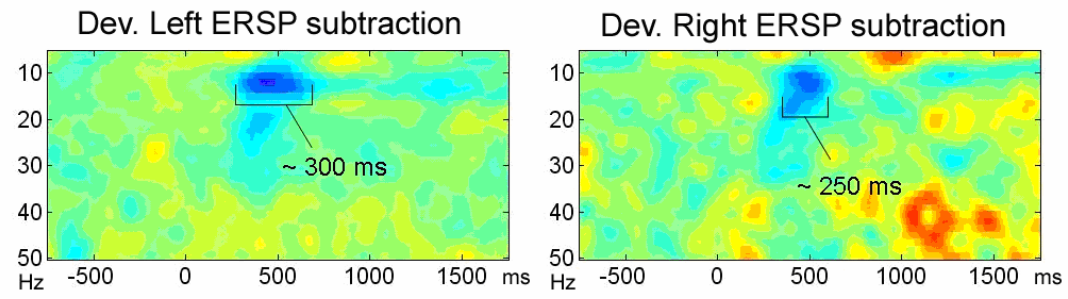

Figure 3-10: The differences between mu blocking in motion and motionless conditions, which were obtained by subtracting motionless ERSP (right panels of Figure 3-9) from the motion ERSP (left panels of Figure 3-9). The ERSP difference images show a brief (250~300 ms) alpha-band power suppression, indicating that the mu blocking occurred earlier in Motion-Deviation than in Motionless-Deviation.

3.4 Discussion

In this study, we recorded and analyzed un-averaged single-trial EEG data in 31 driving experiments from 10 volunteer drivers under two different driving conditions -- motion and motionless. The hexapod motion platform that simulated driving events allowed us to study neural correlates of kinesthetic stimuli, which is difficult, if possible, to study in regular EEG laboratories. We performed ICA to separate the EEG contributions of distinct brain processes to explore their individual and joint event-related dynamics following Stop-Go and deviation events through ERP differences and time-frequency analysis (ERSP). The 9 independent component clusters here identified by their similar scalp projections and activity spectra resemble classes of EEG phenomena long described by neurologists from observations of paper data displays such as central and lateral alpha, left and right mu, and frontal-midline theta rhythms. Alpha power of the mu component cluster was strongly blocked (~-5dB) around the peak of platform movement in Motion-Stop and Motion-Go events. A sharp negative was found in the central midline component cluster only in

Motion-Deviation events. We believe that these two features were induced by kinesthetic stimuli.

3.4.1 Phenomenon in Mu Component

Mu rhythm (μ rhythm) is an EEG rhythm recorded usually from the motor cortex of the dominant hemisphere. It is also called arciform rhythm given the shape of the waveforms. It is a variant of normality, and it can be suppressed by a simple motor activity such as clenching the fist of the contra lateral side, or passively moved (Thilo et al., 2003; Loose et al., 2002; Parker et al., 2001). Mu is believed to be the electrical output of the synchronization of large portions of pyramidal neurons of the motor cortex which control the hand and arm movement when it is inactive.

Deviation events involved subject responses to steer the vehicle back to the cruising position, thus it is expected that mu power would be blocked following deviation events. Our results also showed unexpected strong mu blocking in response to Motion-Stop and Motion-Go events in which no action was involved, suggesting kinesthetic stimuli could also induce mu blocking. Following deviation events, mu power was strongly blocked in both motion and motionless conditions (cf. Figures 3-9 and 3-10). Mean subject RT indexed by the first steering action in response to Motion-Deviation events leads that in response to Motionless-Deviation events by about 50 ms. Thus, we expect that the latency of mu blocking in Motion-Deviation events would lead that in Motionless-Deviation events by a comparable length. However, Figure 3-10 reveals that the mu-blocking latency discrepancy between the two conditions is about 250~300 ms, which could not be attributed entirely to the subject RT latency difference. Mu blocking thus appears associated with kinesthetic stimuli delivered to the drivers. In short, long-lasting mu blocking following deviation events began with the EEG brain dynamics induced by kinesthetic stimuli, followed

by marked mu power decrease associated with subject motor actions. Table 3-1 gives us the information that response time in Motion-Deviation events was only 50 ms faster than in Motionless-Deviation events. By these two results we discovered 200~250 ms duration which was not related to steering action.

3.4.2 Phenomenon in Central Midline Component

The central midline component cluster exhibits a sharp negativity in averaged ERP following Motion-Deviations, but the negativity is missing from the ERP following Motionless-Deviations. The mean ERP in deviate-to-right and deviate-to-left conditions was almost identical. ERP images also show a weaker negative ERP time-locked to subjects' reactions (the black line in the ERP image), which again is comparable following Motion-Deviation and Motionless-Deviation events. Response time in Motion-Deviation events was approximately 50 ms shorter than that in Motionless-Deviation events (as shown in Table 3-1), consistent with a previous report (Wexler et al., 2001) which showed that the absence of motion information increased response times to external movement perturbations.

The sharp negativity in the ERP of the central midline component cluster is also consistent with previous VESTEP studies of Elidan et al. (1982, 1984, & 1987). They showed a negative potential near Cz or forehead, induced by external kinesthetic stimulus. They did not, however, report any mu blocking in response to the kinesthetic stimuli, which to the best of our knowledge has never been reported in the past. The reason is due at least in part to the fact that our experimental environment, which combined visual and vestibular interaction and driver response, was more complicated and realistic than the experimental setups used in previous studies.

3.4.3 EEG Alpha Activity related to Drowsiness

Traditionally, EEG alpha band was used as an indicator of drowsiness estimation during driving (Lin et al., 2005; Eoh et al., 2005). Alpha power has been reported to index the level of drowsiness in attention-sustained experiments in a laboratory setting. In this study, our results showed that alpha-band activity varies during driving, especially when the vehicle is moving and delivers kinesthetic stimuli to the drivers and passengers, which might confound the fatigue-related alpha power changes in driving. Thus, more care must be taken to examine the validity of using alpha power to index drowsiness level in real driving.

Our experiment results show that kinesthetic stimulus during driving induces (1) Mu blocking in the somatomotor components, and (2) Sharp negative ERP in central midline components. The mu blocking appeared to be induced by two types of stimuli successively. When the subjects received kinesthetic inputs, their alpha activities in the left and right mu components were blocked. After a short period, the subjects made an adjustment to balance them, inducing a secondary mu blocking. The alpha power variation induced by the motion of the vehicle might interfere with the estimation of the driving cognitive state based on the fluctuations in the alpha power spectra.

Furthermore, negative ERP was found in central midline components following kinesthetic stimulus onsets. These results demonstrate that multiple cortical EEG sources respond to driving events distinctively in dynamic and static/laboratory environments. A static driving simulator could not induce some cognitive responses that are actively involved in real driving. We also reported that the absence of driving motion will increase the reaction time to external perturbations by studying the response time in deviation events. Thus a driving simulator with a motion platform is crucial to studying event-related brain activities involved in real driving.

4. EEG Activation under Different Cognitive States

4.1 Introduction

The growing number of traffic accidents had become a serious concern to the society in recent years. Accidents caused by driver's drowsiness behind the steering wheel have a high fatality rate because of the marked decline in the driver's abilities of perception, recognition and vehicle control abilities while being sleepy. For instance, the National Highway Traffic Safety Administration (NHTSA) conservatively estimates that 100,000 police-reported crashes are the direct result of driver fatigue each year. This results in an estimated 1,550 deaths, 71,000 injuries and $12.5 billion in monetary losses. The National Science Foundation (NSF) also reported in 2002 that 51% of adult drivers had driven a vehicle while feeling drowsy and 17% had actually fallen asleep. Preventing traffic accidents caused by drowsiness is highly desirable but requires techniques for continuously monitoring, estimating, and predicting the level of alertness of drivers and delivering effective feedbacks to maintain their maximum performance (Pilutti and Ulsoy, 1999). Therefore, we demonstrated an EEG-based drowsiness estimation method in long-term driving in this chapter. In our past research, we had already found the parietal and occipital brain sources were highly correlated with drowsiness via ICA-based signal process (Lin et al., 2005 & 2006). The method combined ICA, EEG log band power spectrum, correlation analysis, and linear regression models to indirectly estimate driver's drowsiness level. Here, we use the same method to estimate subject drowsiness level, except we employ MEMS sensors rather than conventional wet ones to acquire continuous EEG data to demonstrate the potential uses of the MEMS sensors during long and routine recordings in the VR-based dynamic driving environment.

In realistic environment, it is not humane and convenient to acquire the EEG

signal with skin preparation even it had better performance. Using electrolytic gel is not only uncomfortable and inconvenience, but also can cause itchy feeling, and sometimes make skin red and swollen during long-term EEG-measurement. Hence, we also have developed an EEG-based drowsiness estimation algorithm that consisted of signal acquisition, power spectrum estimation, Principal Component Analysis (PCA)-based signal process, and multivariate linear regression to estimate the driver's drowsiness level in the VR-based dynamic driving environment.

4.2 Experimental Setup

Ten subjects (ages from 20 to 40 years, 29.8±5.9 years old) participated in the VR-based highway driving experiments. To maximize the opportunities to get valuable data for our study, all driving experiments were conducted in the early afternoons after lunch. Statistics (Jung et al., 1997; Makeig and Jung, 1995) showed that people often get drowsy within one hour of continuous driving during these periods, indicating that drowsiness is not necessarily caused by long driving-hours. The driving speed is fixed as 100 km/hr and the car is randomly and automatically drifted away from the center of the cruising lane to mimic the consequences of a non-ideal road surface. On the first day, participants were told of the general features of the driving task, completed necessary informed consent material, and then started with a 15 to 30-minute practice to keep the car at the center of the cruising lane by maneuvering the car with the steering wheel. Subjects reported this amount of practice to be sufficient to reach a performance asymptote on the task. After practicing, participants wore wired EEG cap with electrodes and began 1-hour lane-keeping driving task. Participants returned on a different day to complete the other 1-hour driving session for cross-session test. While the subject was alert in the experiment, his/her response time was short and the deviation of the car was small; otherwise the

subject's response time and the car deviation would be slow and long. In this driving experiment, the VR-based freeway scene showed only one car driven on the road without any other event stimuli to simulate a monotonous and unexciting task that could easily make drivers fallen asleep.

The flowchart of data analysis for estimating the level of drowsiness based on the EEG power spectrum is shown in Figure 4-1. For each subject, after collecting EEG signals and driving deviation in 1-hour simulated driving session, the EEG data were first preprocessed using a simple low-pass filter with a cut-off frequency of 50 Hz to remove the line noise and other high-frequency noise. Then, we applied ICA to decompose EEG-signals into temporally independent stationary sources and calculated the moving-averaged log power spectra of all ICA components.

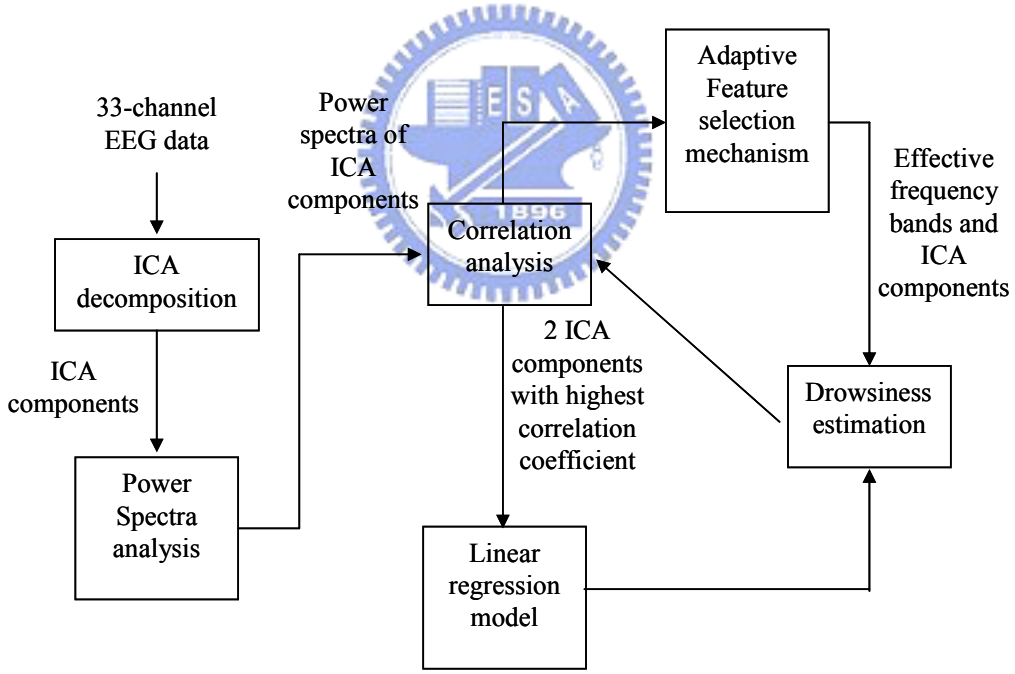

Figure 4-1: Flowchart of the drowsiness detection system

In general, the drowsiness-related regions are mainly in the parietal and occipital lobes. If we acquire the EEG signal from these haired regions of the hindbrain to detect drowsiness level in realistic environment, it is uncomfortable and inconvenient

to acquire the EEG signal from the conventional gel-based sensors on the scalp. To overcome this limitation, we employ the self-stabilized MEMS sensor to replace the conventional ones. The self-stabilized MEMS sensor is expected to circumvent the high impedance characteristics of the stratum corneum (SC) and then skin preparation and electrolytic gel application are not required. Due to the limitation of the current MEMS technology, self-stabilized MEMS sensor is not sufficient to penetrate human hairs to contact stratum germinativum (SG) or even SC. The hair elasticity also makes it difficult to fix the sensor on the scalp. Therefore, the self-stabilized MEMS sensors in this study are placed at non-hairy sites, such as Fp1 and Fp2 on the forehead to on-line estimate the driver's drowsiness level in real-world application.

4.2.1 Experimental Environment

A VR-based dynamic driving simulation environment is designed and built for interactive driving experiments. It includes three major parts: (a) the 3D highway driving scene based on the virtual reality technology, (b) the driving cabin simulator mounted on a 6-DOF dynamic Stewart motion platform (as shown in Figure 2-1 (a) & (b)) and (c) the EEG acquisition system with 13-channel sensors (as shown in Figure 4-2).

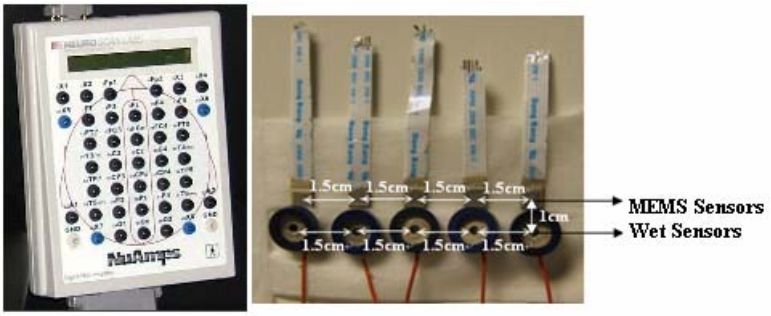

Figure 4-2: A VR-based dynamic driving environment for interactive driving experiments

Acquired EEG signals are analyzed by power spectral density analysis, PCA-based signal processing, and linear regression model to estimate subject's driving performance as shown in Figure 4-3. The subject's performance is defined as the deviations between the center of the vehicle and the center of the cruising (3rd) lane. While the subject was alert in the experiment, his/her response time was short and the deviation of the car was small; otherwise the subject's response time and the car deviation would be slow and long. In this driving experiment, the VR-based freeway scene showed only one car driven on the road without any other event stimuli to simulate a monotonous and unexciting task that could easily make drivers fallen asleep. These physiological and behavioral data are continuously and simultaneously measured and recorded by the WTK program and the acquisition system.

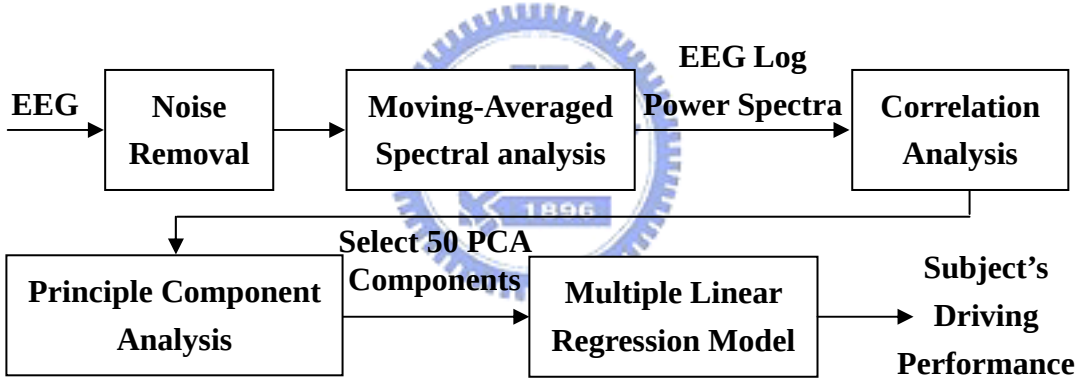

Figure 4-3: Flowchart for processing the EEG signals. (1) A low-pass filter was used to remove the line noise and higher frequency (>50Hz) noise. (2) Moving-averaged spectral analysis was used to calculate the EEG log power spectrum of each channel advancing at 2-sec steps. (3) Two EEG channels with higher correlation coefficients between subject's driving performance and EEG log power spectrum were further selected. (4) PCA was trained and used to decompose selected features and extract the representative PCA-components as the input vectors for the linear regression models (LRM). (5). LRMs were trained in one training session and used to continuously estimate the individual subject's driving performance in the testing session.

The time series of recorded driving performance were smoothed using a causal 90-s square moving-averaged filter (Sterlade, 1993; Treisman, 1984) advancing at 2-sec steps to eliminate variance at cycle lengths shorter than 1-2 minutes since the driving performance tended to vary irregularly with cycle lengths of 4 minutes and longer (Jung et al., 1997; Makeig and Jung, 1995). The EEG data recorded by the MEMS (or wet) electrode pairs were first preprocessed using a simple low-pass filter with a cut-off frequency of 50 Hz to remove the line noise and other high-frequency noise. After moving-average power spectral analysis, we obtained EEG log power spectrum time series for the 5 MEMS (or wet) electrodes. Then, we applied Karhunen-Loeve Principal Component Analysis (PCA) to the resultant EEG log spectrum betweem 1 and 40 Hz to extract the directions of largest variance for each session. Projections of the EEG log spectral data (PCA components) along the subspace formed by the eigenvectors corresponding to the largest 50 eigenvalues were used as inputs to a multiple linear regression model (Chatterjee, 1986) for each individual subject to estimate the time course of his/her driving error (Bishop, 1995). Each model was trained using the features extracted only from the training session and tested on the data from a separate testing session.

4.2.2 EEG Data Acquisition

Figure 4-4 shows the placements of five MEMS/conventional sensor pairs at the frontal locations. The first and fifth MEMS sensors are placed at Fp1 and Fp2 according to the international 10-20 electrode placement system (Thakor, 1999). We also placed three additional MEMS sensors evenly spaced between these two MEMS sensors and labeled them as MEMS2, MEMS3, and MEMS4. Corresponding conventional wet electrodes were placed 1 cm above the MEMS EEG sensors (cf. Figure 4-2). The contact impedance between the MEMS/wet electrode and skin was

calibrated to be less than 5 kΩ. The EEG was recorded from these 5 MEMS and 5 wet electrodes, referenced against linked mastoids (A1, A2) by the Neuroscan NuAmps Express system (Compumedics Ltd., VIC, Australia, as shown in Figure 4-2), band-passed between 0.5 and 100Hz with a 60Hz notch filter, and recorded with 16-bit quantization level at a sampling rate of 500 Hz and then down-sampled to 250 Hz for the simplicity of data processing.

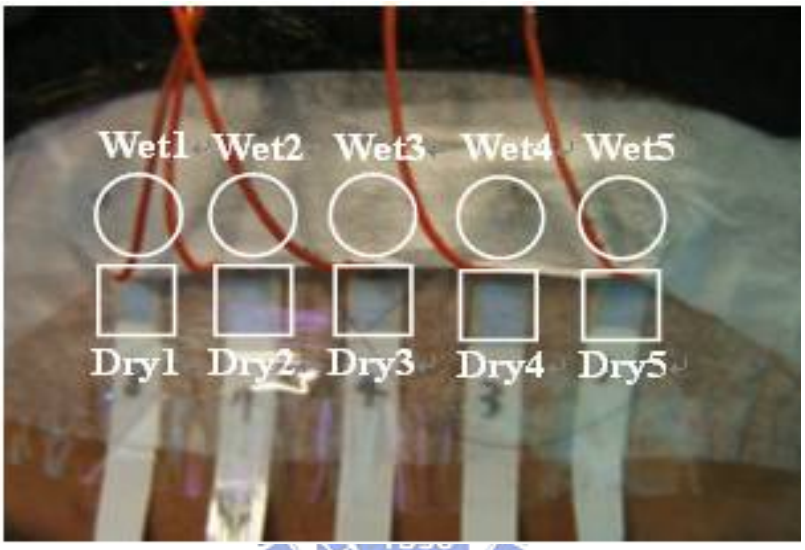

Figure 4-4: Forehead positions of conventional wet electrodes (circle) and MEMS EEG sensors (square)

4.2.3 Lane Keeping Driving Task

In the long-term driving, the car cruised with a fixed velocity of 100 km/hr on the VR-based highway scene and it was randomly drifted either to the left or to the right away from the cruising position with a constant velocity. The subjects were instructed to steer the vehicle back to the center of the cruising lane as quickly as possible. Figure 4-5 shows the time course of a typical deviation event that embedded in the long-term lane-keeping driving task.

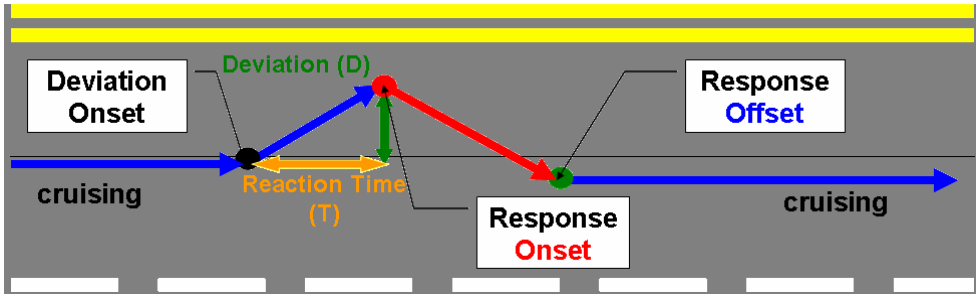

Figure 4-5: An example of the deviation event. The car cruised with a fixed velocity of 100 km/hr on the VR-based highway scene and it was randomly drifted either to the left or to the right away from the cruising position with a constant velocity. The subjects were instructed to steer the vehicle back to the center of the cruising lane as quickly as possible.

Firstly, we need to quantify the volunteer's drowsiness level in this experiment. When subjects fall drowsy, they often exhibits relative inattention to environments, eye closure, less mobility, failure to motor control and making decision (Brookhuis et al., 2003). Hence, the vehicle deviations were defined as the subject's drowsiness index. The VR-based four-lane straight highway scene was applied in the experiment. Figure 4-6 shows an example of the driving performance represented by the vehicle deviation trajectories.

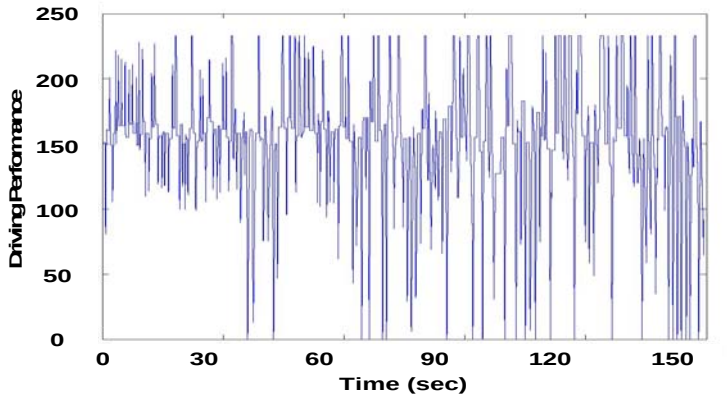

Figure 4-6: An example of the driving performance that represented by the digitized vehicle deviation trajectories

4.3 Experimental Results

In order to demonstrate the potential applications of the MEMS electrodes for long and routine EEG recording in operational environments, we investigated the quality of the EEG signals recorded by the MEMS EEG sensors placed at *Fp1* and *Fp2* for estimating subjects' drowsiness in a sustained-attention driving experiment. The EEG signals recorded by five MEMS sensors were fed into an EEG-based drowsiness estimation system (Lin et al., 2005) as shown in Figure 4-3 to estimate driver's driving performance, an indication of driver's drowsiness level.

4.3.1 Comparison Performance between MEMS-based and Standard Wet Sensor

Figure 4-7 plots the raw EEG signals measured by the proposed MEMS EEG sensors and wet electrode pairs (only the leftmost and rightmost MEMS/wet pairs are shown here). As can be seen, the EEG signals recorded by the MEMS sensors are extremely comparable to those obtained by the corresponding wet electrodes.

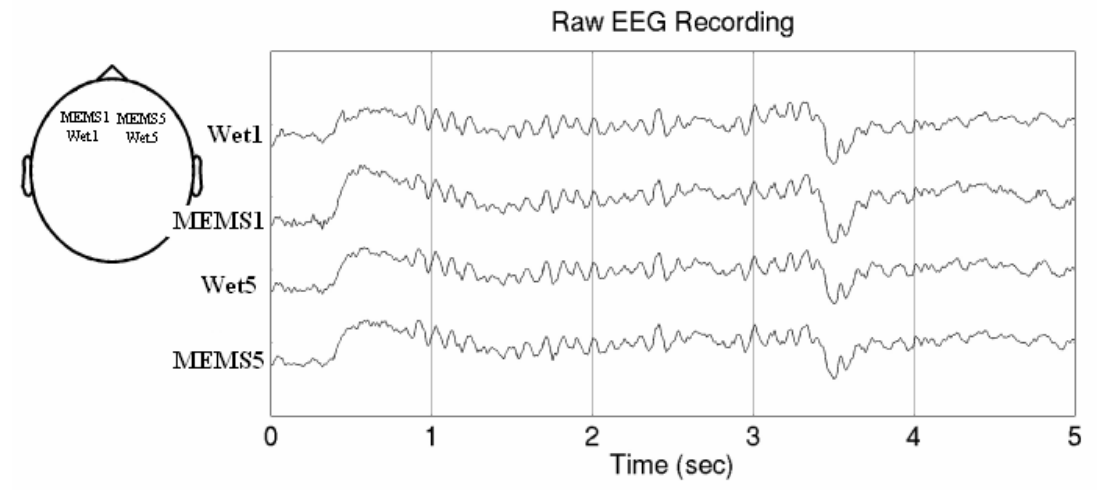

Figure 4-7: Raw EEG Data Recording by MEMS sensors and Standard Wet Sensors

Figure 4-8 over-plots the EEG power spectra of 5 MEMS/wet sensor pairs. As it can been seen, they are extremely similar especially in low frequency bands (1-30Hz),

indicating that the signals obtained by proposed MEMS EEG sensors matched well with the EEG signals recorded by the conventional wet electrodes.

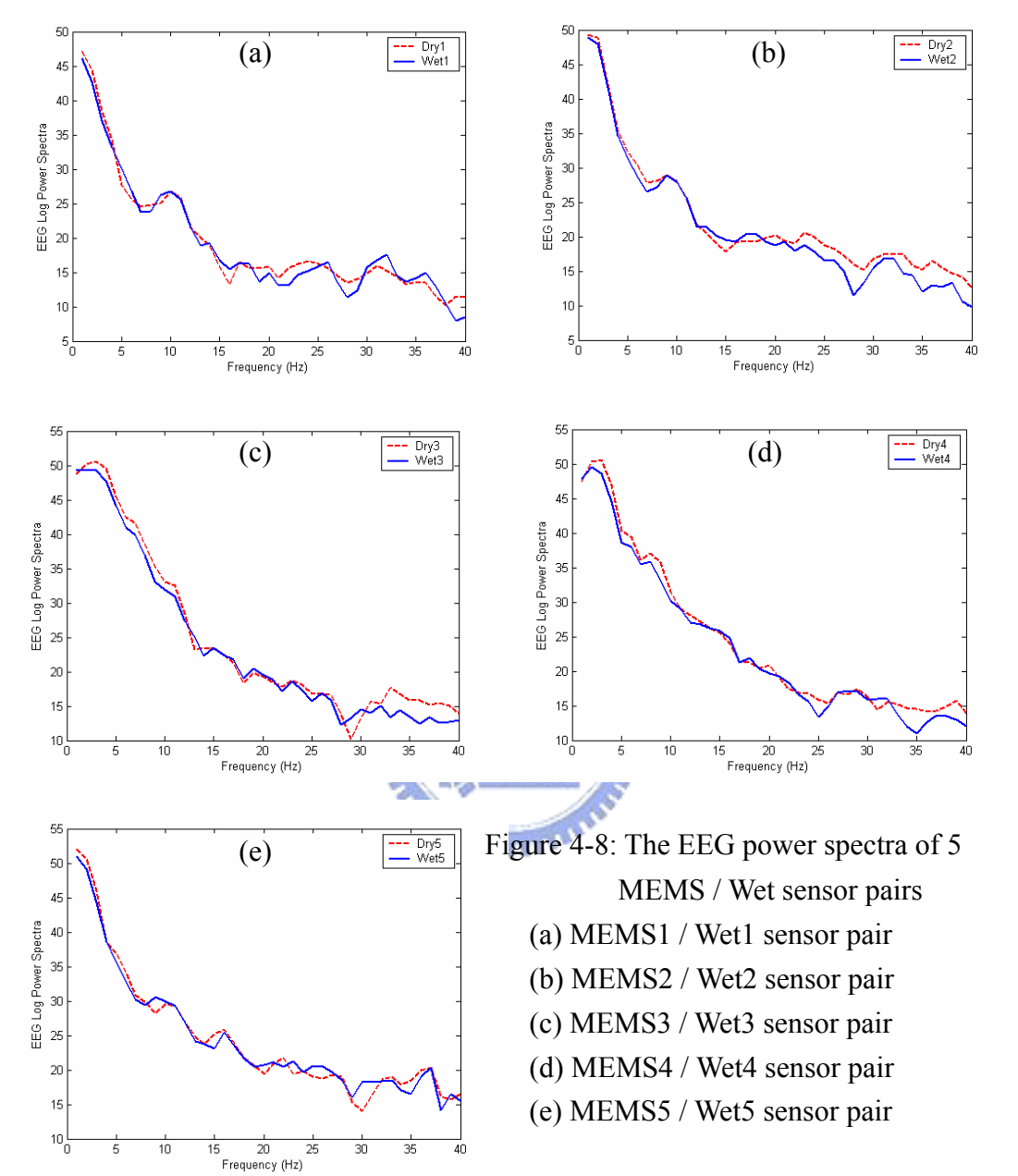

Figure 4-8: The EEG power spectra of 5 MEMS / Wet sensor pairs
(a) MEMS1 / Wet1 sensor pair
(b) MEMS2 / Wet2 sensor pair
(c) MEMS3 / Wet3 sensor pair
(d) MEMS4 / Wet4 sensor pair
(e) MEMS5 / Wet5 sensor pair

4.3.2 Correlation Analysis Results

The correlation coefficients between the subject's driving performance and the log power spectra of all ICA components at each frequency band are further evaluated to form a correlation spectrum. The normalized log sub-band power spectra of top two ICA components with the highest correlation coefficients in some critical bands are

further selected as the input features of the conventional linear regression model to estimate the individual subject's drowsiness level. Figure 4-9 shows the correlation of driving performance and EEG power spectra from the different two subjects. We can easily find that alpha band (8-13 Hz) is highly correlated with drowsiness. These results are consistent with the related studies (Jung et al., 1997; Makeig and Jung, 1996) and alpha band will be a good indicator to detect drowsiness level.

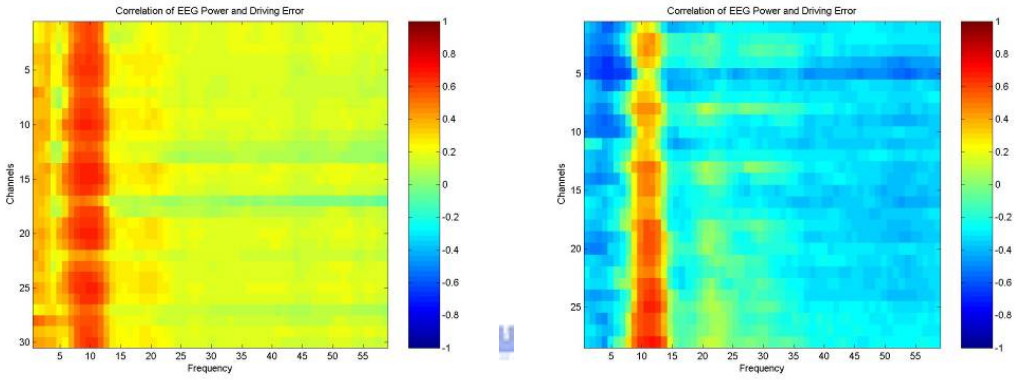

Figure 4-9: Correlation of driving performance and EEG power spectra from the different two subjects

Table 4-1 shows the scalp topographies and spectrum correlation of each subject between driving performance and ICA power spectra of the top two ICA components. The correlations are particularly strong at central and posterior areas, which are consistent with related studies in the driving experiments (Makeig and Inlow, 1993; Makeig and Jung, 1996). The relatively high correlation coefficients near θ-band or α-band may be suitable for drowsiness estimation, as the subject's cognitive state might fall into stage one of the non-rapid eye movement sleep. As can been seen that the best drowsiness-correlated components (best matching) differ in each subject, in general their scalp topographies are all within the ambit of central lobe to occipital lobe.

Table 4-1: Correlation spectra between smoothed driving errors and ICA power spectra of first 2 ICA components of each subject

	SUBJECT1	SUBJECT2	SUBJECT3	SUBJECT4	SUBJECT5
DROWSINESS RELATED ICA COMPONENTS	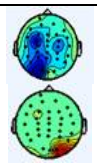	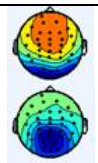	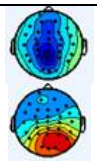	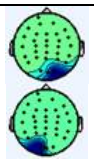	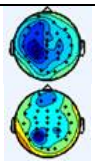
Freq. Bands	5 ~ 9 Hz	8 ~ 12 Hz	10 ~ 14 Hz	4 ~ 8 Hz	8 ~ 12 Hz
	SUBJECT6	SUBJECT7	SUBJECT8	SUBJECT9	SUBJECT10
DROWSINESS RELATED ICA COMPONENTS	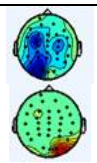	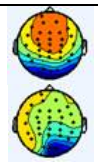	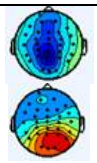	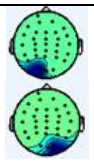	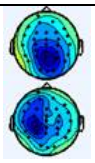
Freq. Bands	4 ~ 8 Hz	5 ~ 9 Hz	9 ~ 13 Hz	7 ~ 11 Hz	10 ~ 14 Hz

4.3.3 Drowsiness Estimation Results

Figure 4-3 shows the flowchart of the EEG-based drowsiness estimation algorithm. EEG signals are analyzed by power spectral density analysis, PCA-based signal processing, and linear regression model to estimate subject's driving performance. Figures 4-10 to 4-13 compare the drowsiness-estimation performance obtained by MEMS EEG sensors and wet electrodes in the sustained-attention driving tasks. They show the minute scale fluctuation of the each driver's driving performance index in 1-hour driving session. In each figure, the blue and red traces represent the acquired and estimated driving errors, respectively, and all of these figures are the results on the testing data.

Figures 4-10(a) and (b) show the estimated driving error in Session #2 of Subject 1 using the EEG signals recorded by the conventional wet electrodes and the MEMS EEG sensors, respectively. The estimators were trained with the EEG signals from Session #1 to estimate the driving error of Session #2 of Subject 1 (the blue traces in Figure 4-10). Conversely, Figures 4-11 (a) and (b) show the estimated driving error of Subject 1 using EEG data from Session #2 as the training dataset and those from

Session #1 as the testing dataset.

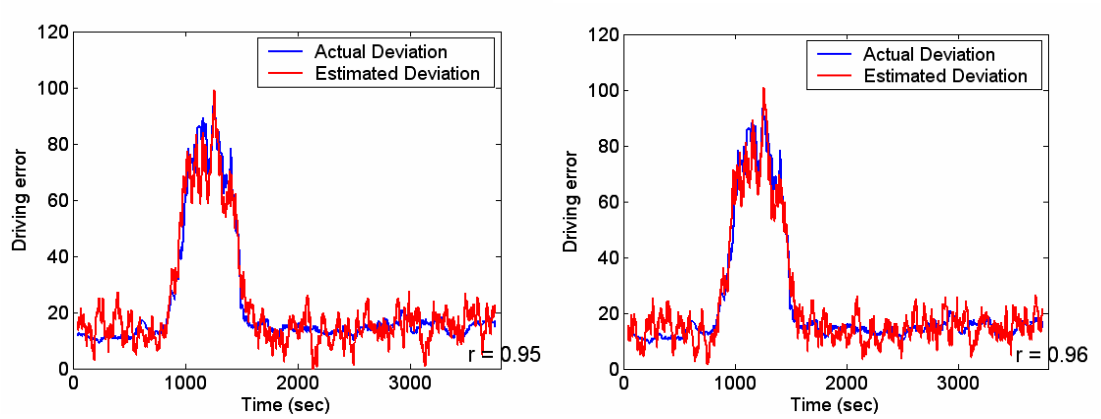

(a) (b)

Figure 4-10: Estimated and actual driving error of Session #2 of Subject 1 using the EEG signals recorded by (a) the conventional wet electrodes and (b) MEMS EEG sensors, respectively. The estimators were trained with the EEG signals from Session #1 to estimate the driving error of Session #2 (the blue traces).

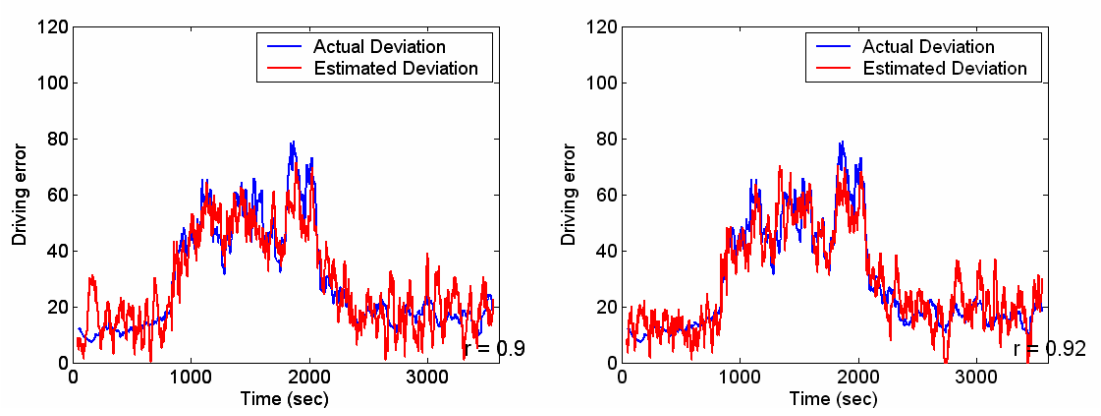

(a) (b)

Figure 4-11: Estimated and actual driving error of Session #1 Subject 1 using the EEG signals recorded by (a) the wet and (b) MEMS electrodes, respectively. The estimators were trained with the EEG signals of Session #2 to estimate the driving error of Session #1 (the blue traces).

Similarly, Figures 4-12 and 4-13 show estimated and actual driving errors made by another subject (Subject 2). Table 4-2 shows the comparison results of correlation coefficient between the actual and estimated driving error time series using MEMS sensors and conventional wet sensors for 5 different subjects.

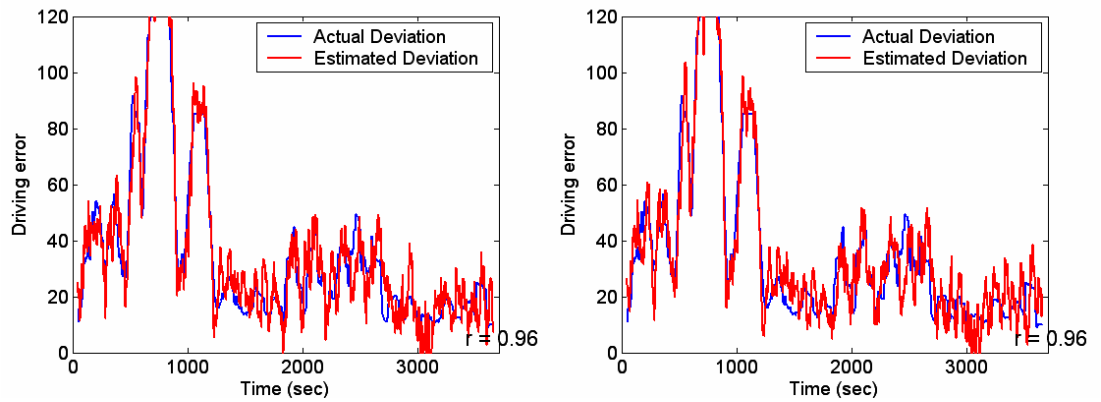

(a) (b)

Figure 4-12: Estimated and actual driving error of Session #2 of Subject 2 using the EEG signals recorded by (a) the wet and (b) MEMS electrodes, respectively. The estimators were trained with the EEG signals from Session #1 to estimate the driving error of Session #2 (the blue traces).

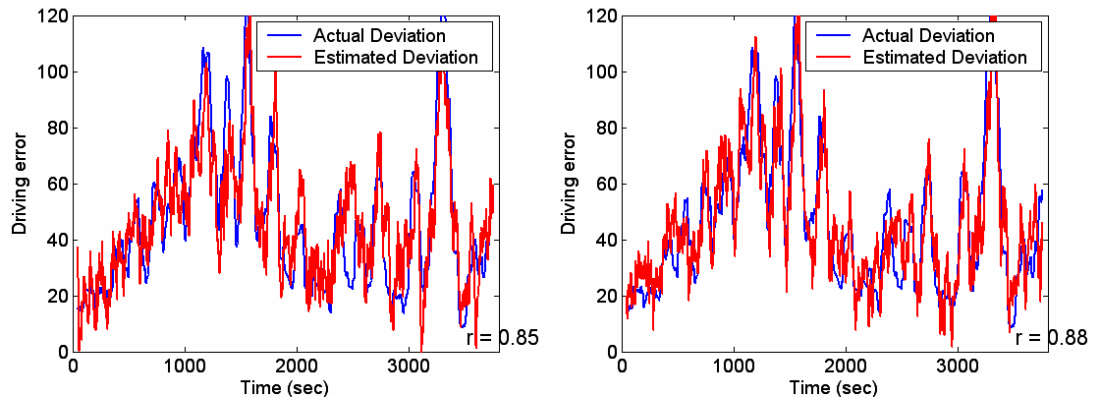

(a) (b)

Figure 4-13: Estimated and actual driving error of Session #1 of Subject 2 using the EEG signals recorded by (a) the wet and (b) proposed electrodes, respectively. The estimators were trained with the EEG signals of Session #2 to estimate the driving error of Session #1 (the blue traces).

Table 4-2: Performance of testing patterns for electrode-skin-electrode impedance (ESEI) measurement

	Session 1 estimates Session 2		Session 2 estimates Session 1	
	Wet sensor	MEMS sensor	Wet sensor	MEMS sensor
Subject 1	0.95	0.96	0.90	0.92
Subject 2	0.96	0.96	0.85	0.88
Subject 3	0.82	0.83	0.84	0.86
Subject 4	0.92	0.94	0.81	0.83
Subject 5	0.85	0.86	0.85	0.88

As can be seen in Figures 4-10 to 4-13 and Table 4-2, the estimated driving errors based on EEG spectra matched well with the actual errors, consistent with our recent report in the same driving tasks using whole-head 32-channel EEG (Lin et al. 2005). The results demonstrated the feasibility of accurately estimating subject task performance based on EEG signals collected from the frontal non-hairy sites. Furthermore, the estimation accuracy based on the EEG collected by the MEMS sensor is comparable to that based on the signals collected by conventional wet sensor, indicating the feasibility of using MEMS sensors that do not require skin preparation or conductive pastes to acquire high-quality EEG signals in operational environments.

In Table 4-2, the correlation coefficient between the two time series (using Session 1 to estimate Session 2) is r = 0.96 of subject 1, r = 0.96 of subject 2, r = 0.83 of subject 3, r = 0.94 of subject 4, and r = 0.86 of subject 5, in the testing session 2. The correlation coefficient between the two time series (using Session 2 to estimate Session 1) is r = 0.92 of subject 1, r = 0.88 of subject 2, r = 0.86 of subject 3, r = 0.83 of subject 4, and r = 0.88 of subject 5, in the testing session 1. The average performance of the estimation system can be reached over 90% by using five self-stabilized MEMS sensors at forehead area.

4.4 Discussion

The lack of availability of EEG monitoring system without use of conductive gels applied to the scalp has long thwarted both military and civilian applications of EEG monitoring in the workplace. In this chapter, MEMS sensors with microprobe array structure bring EEG monitoring to the operational environment without requiring scalp gel or other scalp preparation. Our experimental results demonstrated that the MEMS sensors have advantages in electrode/skin interface impedance, signal intensity and size over the conventional wet sensors. Furthermore, we find that alpha band (8-13 Hz) is highly correlated with drowsiness. It means alpha band will be a good indicator to detect drowsiness level. Hence, we employed the MEMS sensor to collect continuous EEG signals in realistic 1-hour sustained-attention experiments to test the feasibility of using MEMS sensors in operational environments. The EEG-based drowsiness estimation system consists of the MEMS sensor array, power spectrum estimation, PCA-based EEG signal processing, and multivariate linear regression to estimate driver's drowsiness level in a VR-based dynamic driving simulator. The system continuously estimates subject drowsiness level (driving performance) based on the EEG signals measured by the MEMS sensors and parameters derived from the pilot data from the same subject. Our results showed that the MEMS sensors perform comparably to conventional wet sensors placed adjacently, suggesting the practical uses of MEMS sensor in operational environments where skin preparation and messy conductive paste are not feasible or undesirable.

5. Portable Brain Computer Interface in Detecting Drowsiness

5.1 Introduction

The advance in sensor technology and information technology reduces the power consumption of the sensors and make the cost of production cheaper. These trends make it possible to embed sensors in different place or objects to measure a wide variety of physiological signals. A physiological signal monitoring system will be extremely useful in many areas if they are portable and capable of wirelessly monitoring target physiological signals and analyzing them in real time. Biomedical signal monitoring systems have been rapidly advanced with electronic and information technologies in recent years. EEG recordings are usually obtained by placing electrodes on the scalp with a conductive gel or paste, each of which is attached to a wire that is then connected to an external signal acquisition device. The tethering caused by this method of recording prohibits experiments in real operational environments. Furthermore, most of the existing EEG monitoring systems can only record the signals without the capability of automatic analysis. Recently, with the development of embedded system and signal processing technique, there is a tendency to apply the embedded system technique to brain computer interface (BCI). An EEG-based BCI provide a feasible and noninvasive way for the communication between the human brain and the computer (Kalcher et al., 1996; Guger et al., 2001; Cheng et al., 2002; Obermaier et al., 2001). Traditionally, the variations of brain waveforms are measured and analyzed by personal computers (PCs). Due to the inconvenience of PC-based BCI that limits the user's mobility, portable and inexpensive BCI platform—small devices with long battery life that can be carried indoors or outdoors are desired (Bianchi et al., 2003).

There are some studies regarding the portable BCI devices (Gao et al., 2003; Edlinger et al., 2005; Whitchurch et al., 2002). Gao et al. (2003) used steady-state visual evoked potential (SSVEP) to control environmental device, such as TV, video tape recorders, or air-conditioners. A portable pocket PC-based BCI was developed by Edlinger et al. (2005). Whitchurch et al. (2002) developed a wireless system for long term EEG monitoring of absence epilepsy. Obeid et al. (2004) proposed a telemetry system for single unit recording. However, these systems mainly focused on the monitoring hardware but not on real-time analysis. Real-time embedded systems combined with wireless transmission have become a trend of developing diagnosis or homecare systems (Bianchi et al., 2003; Piccini et al., 2004) because they provide a platform to build sensing and inexpensive BCI systems. Many extended applications may be more practicable to implement on the newer platforms whenever the smaller and more powerful devices are developed.

Therefore, we develop a real-time wireless embedded EEG-based BCI system that includes 4-channel physiological signal acquisition, wireless transmission, and a dual-core embedded system with multi-task scheduling in this chapter. The development of a portable and real-time BCI in the virtual-reality-based dynamic driving environment forms the base of investigating brain activities and cognitive state changes with kinesthetic stimuli such as on-line driver drowsiness detection and warning for performance enhancement, investigation of EEG activities of kinesthetic perception. The proposed system employs signal acquisition and amplification units to collect EEG signals and the wireless module for the transmission of the recorded data can overcome the problem of wiring. With the wireless modules, the subject can carry a light sensing module instead of wiring to the analysis system which provides the advantage of mobility. The function of the wireless transmission module is selectable between Bluetooth and a custom-made transmission radio frequency (RF)

mode depending on different applications and locations. Since the processing of the EEG data needs a large number of calculations, the computing power of the embedded system becomes critical when selecting a suitable embedded processor. Therefore, a dual-core processor integrating a DSP and an ARM (advanced RISC machine) processor was used in our embedded system. A multi-task scheduling mechanism was also implemented in the embedded system to enhance the real-time signal processing performance. The proposed structure makes it unique to other system designs in terms of its wireless transmission subsystem and dual-core embedded processors for convenient use and powerful computational capability. Finally, a real-time drowsiness detection method combined with an on-line warning feedback is implemented in the developed BCI system for demonstration. Many traffic accidents on highways are caused by drivers' drowsiness. Our previous studies discovered that some features in human EEG signals are highly related to drowsiness level (Lin et al., 2005 and 2006) and they can be used for estimating driver drowsiness. After the on-line analysis of the EEG data by the multi-task scheduling embedded system, the warning device will be triggered when the drowsiness condition occurs.

5.2 System Architecture

The block diagram of the developed EEG-based BCI system is showed in Figure 5-1, which includes five units: (1) signal acquisition and amplification unit, (2) wireless data transmission unit, (3) embedded signal processing unit, (4) host system for data storage and real-time display, and (5) warning device.

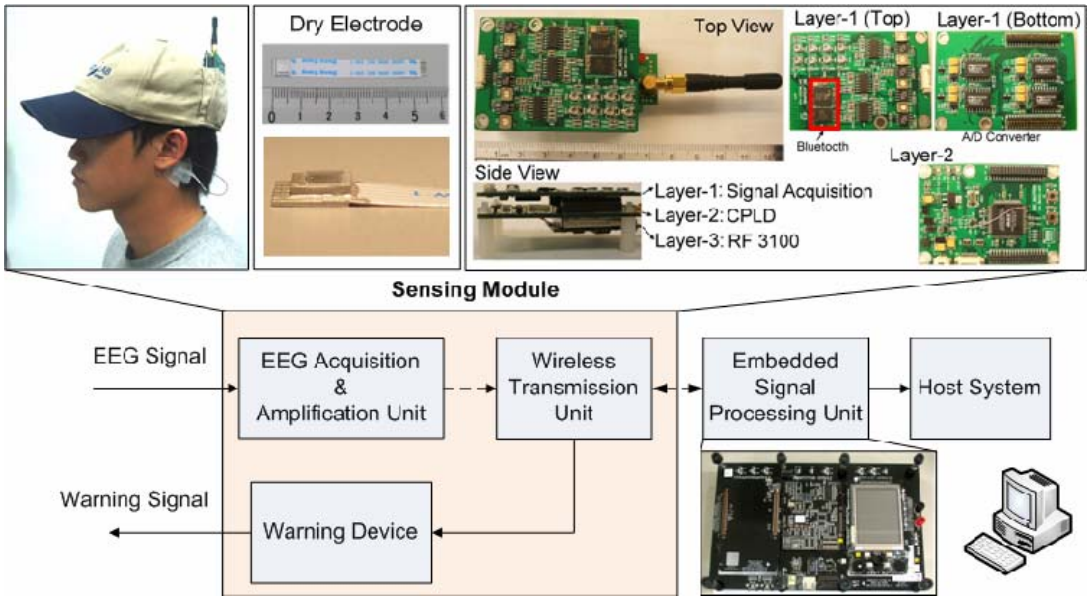

Figure 5-1: The block diagram of the proposed Brain Computer Interface

The three-layer sensing module provides 4-ch biomedical signal acquisition, amplification and wireless transmission functions. The signal acquisition and amplification unit is placed on the top side of layer-1, and the 8-bit A/D converters are designed on the bottom side of layer-1. Layer-2 is the CPLD module that controls A/D and wireless modules. For wireless transmission, RF3100 module is arranged in layer-3, and the Bluetooth module is placed on the top side of layer-1. The size of the sensing module is 4.5cm×6.5cm×2.5cm, and the weight of the module with a Li-ion battery is 51g. The sensing module (including signal acquisition, amplification and wireless units) is designed to operate at 300mA with 3.7-V DC power supply and its power consumption is about 1.11W. The module can continuously operate for at least 45 hours with a commercial 16000mA/h Li-ion battery. Besides, the EEG signal processing unit (OMAP 1510) and the host system (personal computer) is powered with AC.

5.2.1 Signal Acquisition and Amplification Unit

The signal acquisition and amplification unit is applied to measure the EEG signal and to filter out the artifacts as shown in part (a) of Figure 5-2. The EEG amplifying circuit consists of a pre-amplifier (a differential amplifier) with the gain of 100, an isolated amplifier to protect subject, a band-pass filter that was composed of a low-pass filter and a high-pass filter to reserve 1-100Hz signals, a differential amplifier which had the gain of 10 or 50 (that can be chosen by a switch). The gain of the pre-amplifier (100) is larger than the amplifier (a gain of 10) because of the EEG signal is in micro-Volt level, and thus larger amplification is needed before filtering. The capacity we used in the band-pass filter can compensate the DC-offset, thus there are no mechanism designed for the problem. The sensing module that carried by the subjects is designed to operate with a 3.7-Volt DC power supply and the DC voltage can be either supplied by a battery or AC power line. Therefore, a 60Hz notch filter is also included to eliminate the effect of the line noise in case we have to run the system with AC power.

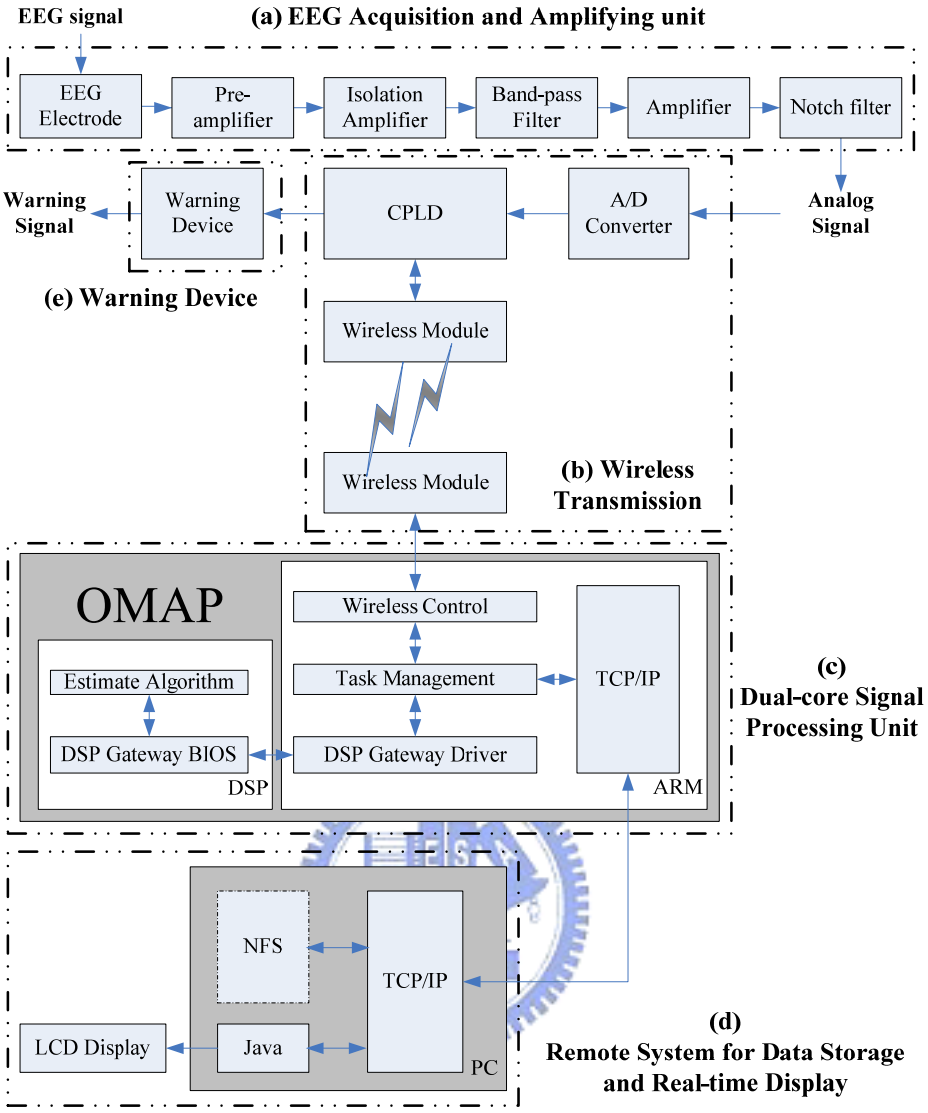

Figure 5-2: The detail architecture of the Brain Computer Interface

5.2.2 Wireless Data Transmission Unit

Part (b) of Figure 5-2 shows the wireless data transmission unit which includes 8-bit A/D converters (parallel output, sampling rate = 768 Hz, AD-7575, Analog Device, Inc.), a Complex Programmable Logic Device (CPLD) and wireless modules. The acquired signal is first converted from analog to digital, and then transmitted through the wireless modules. The ALTERA FLEX10K EPM 7128STC100-7 CPLD is employed to control the A/D converter and encode the data for the wireless modules. Two different transmission methods can be selected in the wireless module

of the designed BCI system according to the transmission distance in applications. Although Bluetooth module is most commonly used in medical/clinical settings where short-distance transmission is required, however, sometimes long-distance transmission is desirable in the settings. In addition to drivers' drowsiness estimation, the system is expected to be applied in various fields such as home cares, clinical physiological signal monitoring, exercise training, etc. Thus, we also integrated a custom-made radio-frequency transmission module with longer operation range in the developed system. RF 3100/3105 (Ancher Technology, Inc.) module is a transparent module that integrates low transmission power and high transmission rate (76800 bps) designs. The comparison of Bluetooth and RF3100/3105 is shown in Table 5-1.

Table 5-1: The Comparison of the Bluetooth and RF 3100/3105

Mode	Bluetooth	RF 3100/3105
Frequency Band	2.4GHz	915MHz
Transmission Distance	10m	200-600m
Transmission Direction	Full-Duplex	Half-Duplex
Modulation Method	Frequency Shift Keying	Frequency Shift Keying
Transmission Power	0dBm (1mW)	12dBm
Interface	UART、USB	UART

The transmission rate is set as 19200 bps only in our final design to prevent transmission error and it can still provide 295 Hz sampling rate for 4-ch signal transmission. This setting is quite enough for general EEG signal acquisition since the most concerned frequency band of EEG signals is during 1~60 Hz. The EEG signals

are recorded at the higher sampling rate to preserve the original signal as well as possible for various applications in addition to drowsiness estimation. Thus the signals are recorded at a higher sampling rate and down-sampled in the EEG signal analysis unit.

5.2.3 Dual-core Processing Unit

It is expected that the portable biomedical devices should provide more advanced functions such as real-time feedback to the users in addition to on-line monitoring. Therefore, more complex processing methods have been proposed for physiological analysis and they will produce more impacts if can be implemented in a real device or product. A dual-core processing unit is adopted as a platform that EEG signal processing methods as well as the intelligent technology can be implemented on it for different applications due to its powerful computation power. The operating core is Texas Instruments (TI) Open Multimedia Architecture Platform (OMAP) 1510, which is composed of an ARM925 processor and a TMS320C55x DSP processor. The DSP core was used to process EEG data and the ARM925 was used to communicate with other devices such as wireless transmission modules and TCP/IP network. The DSP Gateway is used as the cooperation structure for the communication between the two cores since these two cores have different functions as shown in part (c) of Figure 5-2.

DSP gateway is the software that makes ARM core possible to use resource of DSP core by Application Program Interface (API), and works like a small real-time kernel which manages the resource and data flow in the DSP core. With this mechanism, the DSP processor is on only when the system needs to process the EEG data. The Linux operating system (OS) is built to manage the resource of ARM core (Kobayashi and Takahashi, 2003). The functions of ARM core can be divided into three parts: (1) wireless module control, (2) TCP/IP control, and (3) DSP gateway

driver. The ARM core was selected for these tasks due to its excellent interface control ability. The process flow and task distribution in the embedded system are shown in Figure 5-3.

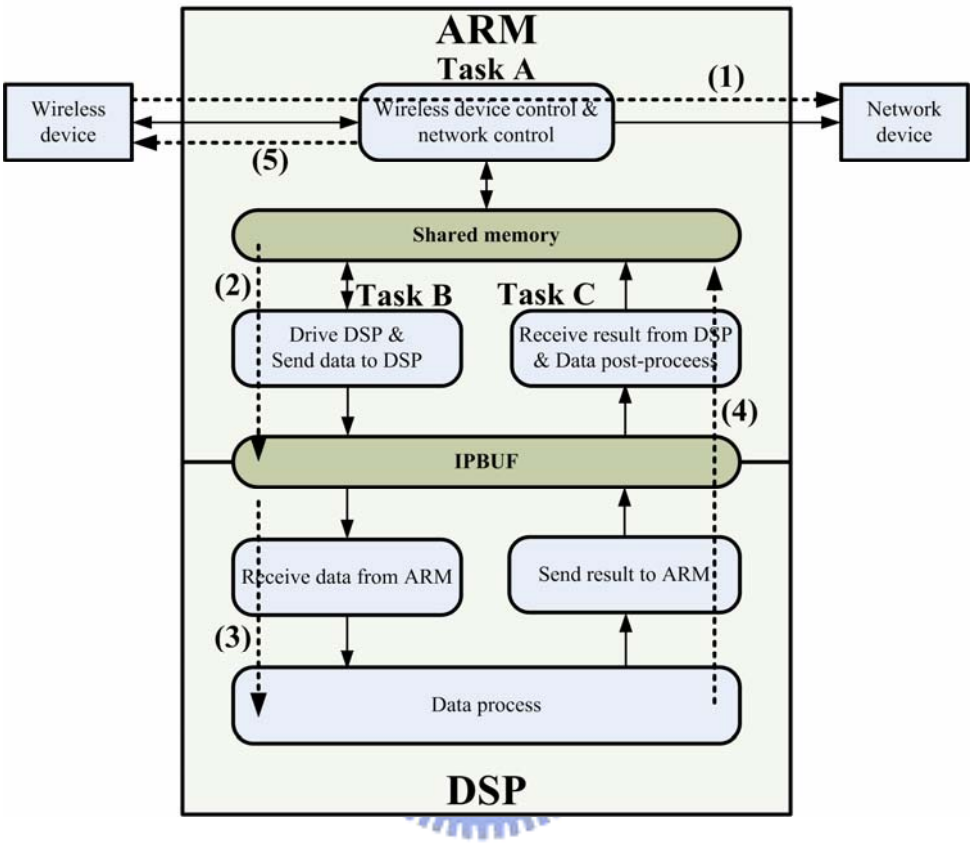

Figure 5-3: Software structure of the embedded system and the data processing flow

There are two processing flows running at the same time including EEG data acquisition and communication and EEG signal processing. The data processing flows are described as follows. (1) After receiving EEG data from wireless device, Task A transmits the data to network. The EEG data are then stored in the shared memory. (2) After the EEG data are stored, Task B enables the DSP module and sends data to DSP. (3) After DSP receives the EEG data, DSP processes the data with Hanning Window and Short-Time FFT analysis. (4) After EEG analysis, DSP sends the result to ARM and ARM performs the other processes and saves the result to the share memory. (5)If

the driver drowsiness is detected through EEG analysis, the embedded system will send the triggering signal to the warning device via wireless transmission.

Since the proposed BCI system is designed to work in real-time, the signal receiving task should continue while EEG signal is on processing. An embedded multi-task scheduling mechanism system is used to manage these tasks and to ensure the accurate sampling rate for EEG signal acquisition and data process/analysis in real time (Liu Jane, 2000). The tasks are divided into three types according to their working frequency: (1) Task A- wireless device and TCP/IP control; (2) Task B- call DSP task and transmit EEG data to IPBUF buffer; (3) Task C- receiving data from IPBUF buffer and further processing of the DSP processed data. The time series diagram of the multi-task scheduling system is shown in Figure 5-4.

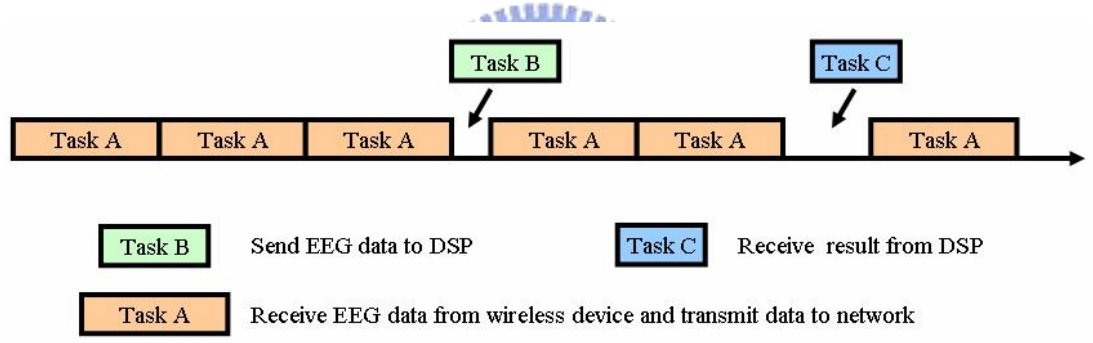

Figure 5-4: Time series diagram of multi-task scheduling mechanism

The working frequency of buffer IPBUF data transmission is much smaller than the working frequency of wireless device and TCP/IP control. Thus we allowed the system continuously to receive signals from the wireless module and output to the display unit through TCP/IP. The system can decide when to process other tasks by itself. With the architecture, the ARM core will not only hold and wait but also keep transmitting data from the wireless module to the display unit when the DSP core is processing the EEG signals. Inter-process communication (IPC) is also an important issue for our scheduling system since the tasks in our system are not completely

independent. In our system, ARM-Linux was used to manage tasks. Linux provides three methods for IPC including: message queue, semaphore, and shared memory. Message queue and semaphore are not efficient enough for the proposed embedded system. Three modified communication methods are employed in the proposed BCI system for inter-process communication: (a) a novel synchronization mechanism, (b) arbitration method, and (c) sharing memory buffer (IPBUF) between processing cores. Traditionally, the synchronization procedure is enabled when two tasks are accessing one memory block at the same time. The memory is blocked when one task is writing or reading on it thus no other task can access to the memory. The synchronization procedure unlocks the blocked memory when the first task finishes writing/reading and then sends a signal to inform other waiting tasks. It's obvious that the mechanism can largely decline the processing speed of the processor. A new synchronization mechanism is designed to deal with the simultaneous memory access by both receiving EEG data from EEG acquisition system (Task A) and sending EEG data to DSP (Task B). When task A is accessing the memory, Task B will be idle and waste some time in waiting. Therefore, we use two blocks of memory with the same size to reduce the waiting time. When Task A is storing EEG data on memory M1, Task B can get the EEG data from memory M2 at the same time. With the modified procedure, these two tasks can execute concurrently and reduce the waiting time caused by synchronization control. Although the method consumes double memory size to complete the procedure, the required extra memory is less than 4K bytes. Besides, we use arbitration flag register instead of semaphore due to that the speed of flag register based on shared memory is the fastest IPC method in Linux platform. In addition, using flag register can reduce the amount of memory needed because one declared variable can contain many flags.

5.2.4 Host System for Data Storage and Real-Time Display

The structure of the host system is shown in part (d) of Figure 5-2. The host system has two functions including data storage and real-time EEG signal display. The data size of continuous EEG recordings is beyond the storage capacity of the embedded system. Thus, we have implemented a network file system to store EEG signals. Additionally, we built a graphic user interface (GUI) to show the bio-medical signals in real-time as shown in Figure 5-6 (c). The connection between the host system and the embedded system is TCP/IP protocol.

5.2.5 Warning Device

The warning device is combined in our system as shown in Figure 5-2 (e). Visual signal and audio signal can be presented to the BCI users as the feedback warning signals. The audio signals are more effective in our prior study for driver drowsiness warning since it is easier to detect audio signals than visual signals for the driver when he/she is drowsy. The efficiency of audio signals with different frequencies: 500Hz, 1750Hz, and 3000 Hz were tested in the prior study and the audio signal of 1750Hz achieves the best results. The triggering signals are sending from the dual-core EEG signal processing unit to the warning device through wireless transmission modules. The RF3100/3105 modules are half-duplex, which means the modules cannot transfer and receive signals at the same time. Since the signals are transmitted as packages, a package of warning signal can be transmitted in the time period between two packages of the acquired EEG signals for transmission. The time period between two packages might be too short for the reverse-direction transmission if the transmission frequency is set too high. To deal with the problem, the transmission frequency is set lower to leave some time duration for the data transmission from the other end.

5.3 Real-time Driver's Drowsiness Detection and Warning

With combining on-line EEG recording and wireless transmission ability, the proposed BCI system is designed for real-time physiological signal analysis. Thus a real-time drowsiness detection method combined with an on-line warning feedback is implemented in the developed BCI system for demonstration. A dynamic operating environment is also built up to test and verify the robustness of the BCI system.

5.3.1 Experimental Design

The virtual-reality (VR) based dynamic driving environment reported in chapter 2 was used to investigate those changes on drivers' cognitive states in long-hour driving tasks. However, the traditional wet electrode requires electrical gel to increase the conductivity between the electrode and the scalp. Thus it takes time for preparation and the subjects need to wash their hair after recording. For the convenience in practical applications, we place five dry electrodes (Chiou et al., 2006) on the driver's forehead and the distance between two near electrodes is 1.5 cm to acquire the EEG signals for the BCI system. The EEG features related to alertness changes can be extracted from EEG signals acquired by the electrodes at the forehead according to our experiments. Therefore, placing electrode array on the forehead is a feasible and convenient strategy for drivers' drowsiness estimation. Six dry electrodes are used to acquire EEG signals from the driver including five electrodes placed on the subject's forehead and one placed behind the subject's left ear. The five electrodes we placed on subject's forehead including a common ground electrode and 4 EEG electrodes. The ground electrode is directly connected to the ground of power supply. The EEG signals we used in further analysis are measured between the 4 EEG electrodes and the reference electrode. The dry electrodes and the sensing module can be embedded in a hat as shown in Figure 5-1. The combination of the dry electrodes

and the sensing module has gradually improved the convenience and the future applicability of the developed system.

5.3.2 Data Processing Flow and Analyzing System Design

The analysis procedure implemented in the dual-core signal processing unit is shown in Figure 5-5. The acquired EEG signals are first down-sampled to 64 Hz to reduce the calculation loading of the system and a 64-points Hanning-window is then applied to smooth the signals. The short-time Fourier transform is used to extract the time-frequency characteristics of the EEG signals and a 90-second moving average filter is applied to eliminate the noise.

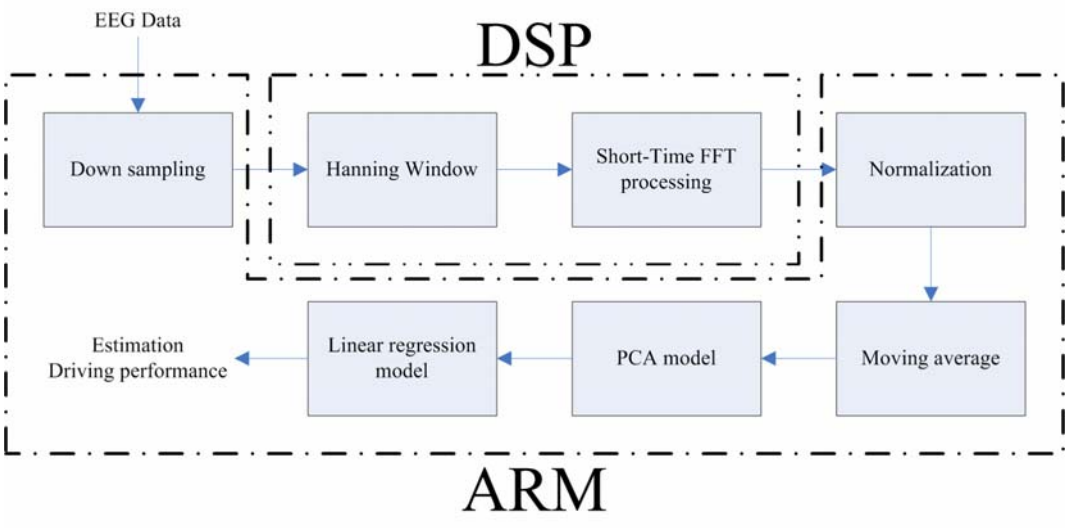

Figure 5-5: Flowchart of the proposed EEG signal analysis procedure

We use principal component analysis (PCA) on the EEG power spectrum to reduce the data dimension and the computational loading of the embedded system. The EEG features (dimension = 20) extracted by PCA are then fed into a linear regression model to estimate the driver's drowsiness levels. The EEG signals collected in the first session were used to construct his/her drowsiness estimation model including the PCA method through off-line training by the PC. The model

including the PCA matrix is then load into OMAP 1510 to process and analysis the subject's EEG signals in the other days in on-line and real-time for testing.

The main tasks of the embedded processor OMAP1510 was to process EEG data, wireless receiver control, and TCP/IP control. Thus we distributed these tasks into DSP core and ARM core to retain satisfied performance. According to the characteristics of the processors, the calculation of driving error estimation needed to process a long period of EEG data, so it was implemented in ARM processor. On the other hand, the Hanning windowing and short-time FFT needs heavy computation and thus implemented in the DSP core to balance the computation load. The remaining processes were implemented in ARM, because they need relatively less computations.

5.4 Experimental Results and Discussion

The feasibility of the proposed BCI system is tested in three aspects. First, we test the basic functions including bio-medical signal amplification/acquisition and wireless transmission of the system. The embedded multi-task scheduling system will then be tested and compared with the system without scheduling. Finally, the accuracy of the embedded drowsiness monitoring system will be evaluated.

5.4.1 Test of the Basic Functions

The basic functions of the developed BCI system should be tested before any further applications. The sub-systems are designed in modules to make the system more flexible for different applications. Thus the test of the system can be divided into two phases, the sub-system testing and the overall-system testing. The acquisition/amplifying unit is tested for its dependability by three steps. First, a sin wave with frequency of 5 Hz and 30uV vibration amplitude generated by the EEG simulator is used for simulation test. Then EEG signals of eye blinking were test

because the amplitude of the signals will be larger and it is easy to be recognized from acquired signal. Finally, we want to measure α wave to confirm the signal we measured is real EEG signal. When subjects take rest and close their eyes, we can continuously measure α wave which with frequency band between 8-12 Hz. Figure 5-6 (b) shows the α wave measured by the developed system.

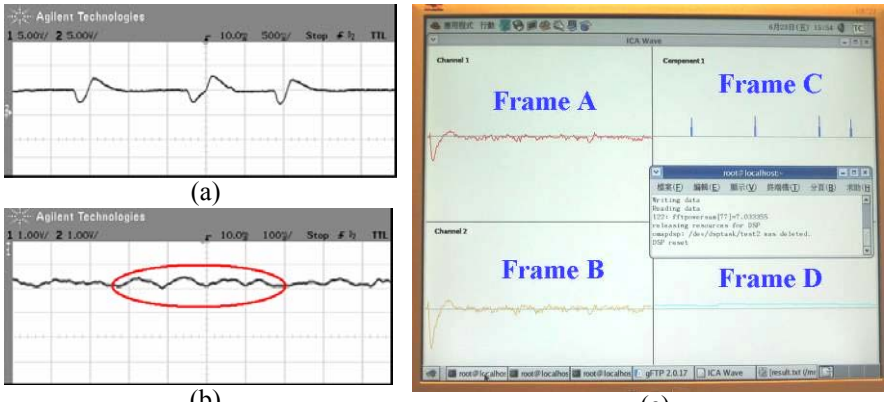

Figure 5-6: Testing results of the acquisition/amplifying unit and the developed GUI monitoring interface

After tested and verified the subsystems, we test and verify the whole system online. In order to show the processed results of our system, we developed a Java graphic user interface (GUI) to receive the processed results of the embedded system by TCP/IP network and plot them on the display screen as shown in Figure 5-6 (c). The left two frames are two-channel EEG raw data (Frame A, B), and the right frames show the estimated drowsiness levels (Frame C, D).

5.4.2 Embedded Multi-Task Scheduling

The multi-task scheduling mechanism was developed to ensure the accurate sampling rate for EEG signal acquisition and data analysis in real time. In order to test the performance of the embedded multi-task scheduling system, two-channel EEG

data with sampling rate of 65Hz were fed to the BCI system. The time consumptions of BCI system executing 1000 cycles of signal processing procedure in DSP with and without embedded multi-task scheduling are compared and the test results are shown in Table 5-2. It takes 2425 seconds to complete the 1000 cycles without multi-task scheduling, whereas the system with multi-task scheduling needs only 1933 seconds.

Table 5-2: The Comparison of the Performance

Execution Time (second)	Considering the time of data receiving		Without considering the time of data receiving	
	Without multi-task scheduling	With multi-task scheduling	Without multi-task scheduling	With multi-task scheduling
1000 cycles	2425	1933	587	95
One cycle	2.425	1.933	0.587	0.095

It is noted that the execution time is mainly used in receiving data. It takes 1838 seconds for the system to receive data which means it takes only 95 and 587 seconds for 1000-cycle data processing with and without multi-task scheduling, respectively. In average, it takes 1.933 second and 2.425 seconds to complete one data processing cycle (the drowsiness level in 2 seconds) with and without multi-task scheduling, respectively. If the time cost of data reception is not considered, the executing time will be reduced from 0.6 second to 0.1 second with embedded multi-task scheduling. As a result, the embedded multi-task scheduling system is useful to reduce the execution time and ensure the correctness of the received data. It takes about 1.933

second to calculate a value of driving error. The result is shown in Frame C of Figure 5-6 (c) as a peak. The time interval between two peaks is about 2 seconds.

5.4.3 Drowsiness Detection

In order to test and verify the feasibility of applying the developed embossed BCI system into practical applications, the drowsiness detection method proposed in chapter 4 was implemented in the BCI system for on-line testing. Two different sessions of EEG signals are acquired in different day for each subject. The EEG data collected in the 1st session is used as training data to construct a driving error estimating system. The EEG data collected from the 2nd session is then applied to the constructed estimating system to predict the drowsiness levels of the driver. The result is shown in Frame C of Figure 5-6 (c) as a peak. The time interval between two peaks is about 2 seconds. The amplitude of the peak represents the estimated driving error calculated by the drowsiness estimating system. The subject is considered drowsy if the value of driving error is bigger than a threshold and the warning device will be triggered. The correlation coefficient between the predicted drowsiness levels and the actual driving error acquired in the second session is calculated as an index of the system performance.

The training and testing results of the drowsiness level estimation for subject 5 is shown in Figure 5-7. The red dash line in Figure 5-7 indicates the drowsiness level estimated by the BCI system and the blue solid line is the acquired driving error. The comparison of the estimating performance for 5 individual subjects is given in Table 5-3. The average correlation between the estimated and the acquired data among 5 subjects can reach to 75%.

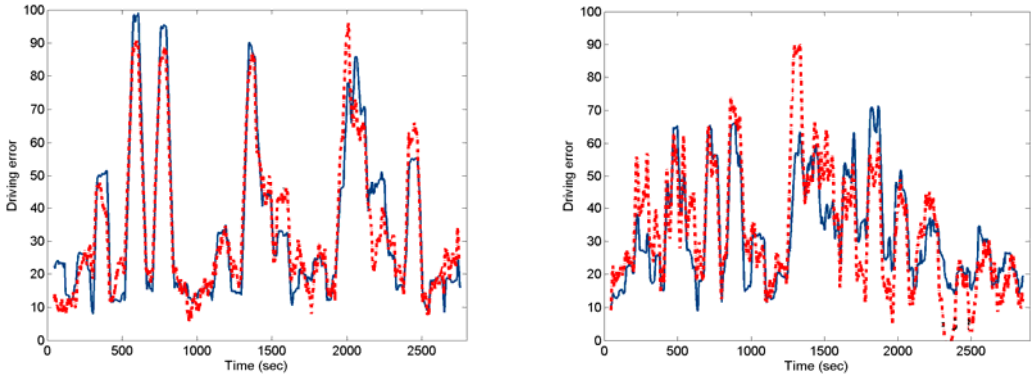

(a) Training result (b) Testing result

Figure 5-7: The training and testing results of the drowsiness level estimation implemented on the embedded BCI system.

Table 5-3. The comparisons of the Estimation Performance

Subject	1	2	3	4	5	Average
Training	97%	96%	86%	95%	93%	92.6%
Testing	77%	85%	78%	72%	81%	78.6%

5.4.4 Comparisons and Discussions

The specifications of the proposed BCI system and the other existing systems are concluded in Table 5-4. Gao et al. (2003) proposed an environmental controller using a BCI technique based on steady-state visual evoked potential and the system consists of a stimulator, a digital signal processor, and a trainable infrared sensing-controller. They applied a FFT and a feature extraction mechanism in DSP to control the electric apparatus. The Graz-brain-computer interface (BCI) (Edlinger et al., 2005) is a cue-based system using the imagery of motor action as the appropriate mental task. Whitchurch et al. (2002) devised a wireless monitoring system based on Bluetooth to enable the physician to monitor the EEG when the patient resumes his/her normal

activity for the reason that the transmission band (2.4GHz) is allowed in hospital. Obeid et al. (2003) developed a 16 channel sensing telemetry system to facilitate multichannel single unit recordings from freely moving test subjects. The 16-channel signals derived from implanted neural electrodes were transmitted through IEEE 802.11b. It only can work for 45 minutes without power supply due to large power consumption.

Table 5-4: Comparison of Brain Computer Interface Systems

BCI System	Gao et al. (2003)	Whitchurch et al. (2002)	Obeid et al. (2003)	Edlinger et al., 2005	Our BCI System
Signal	EEG	EEG	Single unit	EEG/ECG/ EOG	EEG/EMG ECG/EOG
Channels	2	6	16	8	5
Transmission Method	Wire	Bluetooth	WLAN IEEE802.11b	Wire	Bluetooth/ RF
Resolution of A/D	12	12	8	16	8
Sampling Rate (Hz)	200	--	244	256	457
Gain	--	10000	500/1000	--	1000/5000
Filter	4~35 Hz band pass 50 Hz notch	60 Hz low pass	211 Hz high-pass	--	1~100Hz band pass 60 Hz notch
Signal Processing	DSP	Laptop	66MHz AMD Processor	PDA	Dual-Core DSP
Analysis Procedures	FFT and Feature Extraction	--	--	FFT	FFT/PCA Estimation Model

Regarding to the proposed system, we used two different wireless transmission modules to ensure the flexibility of the proposed BCI system since the transmission distance of Bluetooth can only cover 10 meters while the RF module can cover more

than 200 meters. Users can easily switch between the two wireless modules depending on different application environments. Main procedures were implemented in the signal processing unit and the real-time capability is also guaranteed due to the developed embedded multi-task scheduling mechanism. It can also provide on-line warning signals when the abnormal state of uses such as drowsiness in driving appears.

6. Conclusions

EEG has been widely used for both clinical diagnosis and fundamental cognitive neuroscience because its low cost, high temporal resolution and need for the subject to hold still is less stringent than other brain imaging modalities such as functional magnetic resonance imaging (fMRI) and Magnetoencephalogram (MEG). However, compared to other modalities, EEG has long been considered an imaging modality with relatively high noise and low spatial resolution. These technical and methodological issues have limited researchers to explore the applications of EEG in operational environments. Research at our Center has shown EEG to be, by contrast, a rich source of information about ongoing cortical brain dynamics, both local, and distributed, with both millisecond-scale time resolution and a surprising degree of spatial resolution and complexity. The driving force in this dramatic revaluation of the perceived value of EEG imaging is the development and application of more adequate computational methods and models in EEG interpretation. We believe the recent advances in electronics and signal-processing methods have made it the applications of EEG monitoring feasible in the workplace. My research has been to develop hardware and software to push the envelope of today's applications of EEG to monitoring brain dynamics of participants performing ordinary tasks in the workplace.

To this end, in this study, we have constructed a VR-based dynamic driving environment for BCI research by providing subjects kinesthetic stimuli along with the normal visual and/or auditory stimuli. The VR platform incorporates the technologies of information science, mechanism, and control. This Steward Platform provides the user realistic sensations (including vision and motion) of driving and allows subjects to control the mounted vehicle through a steering wheel. This setup

allows us to study high-temporal-resolution event-related brain dynamics following various driving events. We applied ICA to separate the distinct EEG contributions arising from different brain processes to explore their individual and joint event-related dynamics following Stop-Go and deviation events through ERP differences and time-frequency analysis, ERSP. Our results showed that kinesthetic stimulus during driving induce (1) Mu blocking in the somato-motor components, and (2) Sharp negative ERP in central midline components. The mu blocking appeared to be induced by two types of stimuli. When the subjects received kinesthetic inputs, their alpha activities in the left and right somato-motor areas were significantly reduced (blocked). After a short period, the subjects made an adjustment to balance them, inducing a secondary mu blocking. The alpha power variation induced by the motion of the vehicle might interfere with the estimation of the driving cognitive state based on the fluctuations in the alpha power spectra.

Furthermore, negative ERP was found in central midline components following kinesthetic stimulus onsets. These results demonstrate that multiple cortical EEG sources respond to driving events distinctively in the dynamic environment, which could not be found in regular static laboratories because a static driving simulator could not induce some cognitive responses that are actively involved in real driving. We also reported that the absence of driving motion will increase the reaction time to external perturbations These EEG correlates of kinesthetic stimuli might have profound implications for EEG studies. Our results suggested we might need to re-consider the applicability of the findings from so-called ‘well managed’ studies from regular EEG laboratories to the EEG dynamics in the workplace.

In a parallel effort to push the envelope of today's applications of EEG to the workplace, we had successfully developed the wireless embedded BCI system with real-time bio-signals processing ability. The system consists of 4-channel

self-stabilized MEMS sensors, signal acquisition and amplification circuits, a wireless transmission unit, a dual-core signal processing unit, a display and monitoring unit, and a warning device for assessing human physiological and mental information in operational environments. The development of a portable and real-time BCI in the virtual-reality-based dynamic driving environment forms the base of next-generation neuro-imaging modality – mobile high-definition high-definition electromagnetic brain imaging that imaging of participants actively performing ordinary tasks in natural body positions and situations within a real-world environment.

EEG signals were first acquired by signal acquisition and amplification unit, and then transmitted from wireless data transmitter to wireless data receiver. The wirelessly transmitted EEG signals were processed by the data processing unit and the processed results were then transmitted to the sensing system for data storage, real-time display or triggering the warning devices by TCP/IP. A multi-task scheduling procedure was employed in the dual-core signal processing unit to enhance the efficiency of the embedded system and ensure that the BCI system properly works in real-time. A real-time drowsiness detection method combined with an on-line warning feedback was also implemented in the mobile BCI system for demonstration. This research incorporates the several important technologies: (1) a sensing module for signal acquisition, amplification and wireless transmission, (2) a dual-core embedded system for real-time EEG signal processing, and (3) an automatic bio-feedback loop for on-line warning. By combining these technologies, the portable BCI platform has enough flexibility to be applied and adapted to various applications.

Our test results showed that self-stabilized MEMS sensors with microprobe array structure can be used to acquire high-fidelity EEG monitoring in a realistic environment without requiring scalp gel or other scalp preparation. Furthermore, we

have successfully applied this real-time prosthetic system to collect continuous EEG signals in realistic 1-hour sustained-attention experiments to test the feasibility of using self-stabilized MEMS sensors in kinesthetic VR-based driving environment. The system could continuously estimate the drowsiness level of the subjects (with average estimation performance over 90%) by using five self-stabilized MEMS sensors placed at the forehead.

We plan to further optimize the current portable BCI system and test it in real environments. Future directions include: Ultra-low power circuits for portability and optimized computational methods to real-time EEG signal processing. We will implement the BCI in a small unit consisting of advanced EEG amplifiers and software programs that implement our cognitive-state monitoring and transient brain-response detection techniques. During normal operation, the system will estimate a brain-state in real time and will deliver information on significant brain-state changes to the operator in the form of auditory and visual feedback according to the operators' cognitive state and response lapses to critical situations. It will also optimize the information presentation rates and timing according to the operators' cognitive states.

In conclusion, this dissertation describes a design, development and testing of a neural human machine interface/interaction that allows assessment of brain activities of participants actively performing ordinary tasks in natural body positions and situations within a real operational environment. The development of the portable and real-time BCI system can acquire and analyze electroencephalogram (EEG) signals in real-time to monitor human physiological signals as well as cognitive states and, in turn, provide feedbacks to the users when needed. More importantly, this dissertation also discuss the implications of this innovative mobile wireless brain imaging technology in neuroscience and neuro-technology, through three sample studies: (1)

cognitive-state monitoring of participants performing realistic driving tasks in the virtual-reality-based dynamic driving simulator; (2) the efficacy and neural correlates of auditory feedback delivered to participants to maintain participants attention and alertness; (3) the neural correlates of kinesthetic sensation and perception in the dynamic driving simulator.

Results of these studies provide many new insights into the understanding of complex brain functions of participants performing ordinary/routine tasks in a minimum constrained environment. These results also allow a better appreciation of the limitations of normal human performance in repetitive task environments, and may allow more detailed study of changes in cognitive dynamics in brain-damaged, diseased, or genetically abnormal individuals. Furthermore, these findings might be difficult, if ever possible, to obtain in a standard EEG laboratory where participants are asked to limit their eye blinks, teeth clinching, head/ body movements. We, thus, believe this work opens a new chapter in neuro-cognitive human-machine interface/interaction. It will widen the fundamental biomedical and brain science research, and spawns new industry opportunities to provide the solutions of real-life problems.

Reference

Baudonniere P. M., Belkhenchir S., Lepecq J. C., Mertz S. (1999): Otolith-vestibular-evoked potentials in humans: Intensity, direction of acceleration (Z+, Z-), and BESA modeling of generators. *Annals of the New York Academy of Sciences*, vol. 871, pp. 384-386.

Bell A. J. and Sejnowski T. J. (1995): An information-maximization approach to blind separation and blind deconvolution. *Neural Computation*, vol. 7, pp. 1129–1159.

Berthoz A., Israel I., Georges-Francois P., Grasso R., Tsuzuku T. (1995): Spatial memory of body linear displacement: what is being stored? *Science*, vol. 269, pp. 95-98.

Berthoz A. (2000): *The Brain's Sense of Movement.* Cambridge MA: Harvard University Press. 352p.

Bianchi L., Babiloni F., Cincotti F., Arrivas M., Bollero P., and Marciani M. G. (2003): Developing Sensing Bio-Feedback Systems: A General-Purpose Platform. *IEEE Transactions on Neural Systems and Rehabilitation Engineering*, vol. 11, no. 2, pp. 117–119.

Bishop C. M. (1995): *Neural Networks for Pattern Recognition*, Oxford University Press, Oxford.

Brookhuis K. A., Waard D. D., and Fairclough S. H. (2003): Criteria for driver mpairment. *Ergonomics*, vol 46, pp. 433-445.

Cardoso J. F. and Souloumiac A. (1993): Blind beamforming for non Gaussian signals. *IEE Proceedings F in Radar and Signal Processing*, vol. 140, no. 6, pp. 362-370.

Chatterjee S. and Hadi A. S. (1986): Influential Observations, High Leverage Points, and Outliers in Linear Regression. *Statistical Science*, pp. 379-416.

Cheng M., Gao X., Gao S., and Xu D. (2002): Design and Implementation of a Brain-Computer Interface With High Transfer Rates. *IEEE Transactions on*

biomedical Engineering, vol. 49, no. 10, pp. 1181- 1186.

Chiou J.C., Ko L.W., Lin C. T., Jung T. P., Liang S. F., and Jeng J. L. (2006): Using Novel MEMS EEG Sensors in Detecting Drowsiness Application. *Proceedings of IEEE Biomedical Circuits and Systems Conference*, London, United Kingdom, Nov. 29-Dec. 1.

Comon P. (1994): Independent component analysis — A new concept? *Signal Processing*, vol. 36, pp. 287–314.

Edlinger G., Krausz G., Laundl F., Niedermayer I., and Guger C. (2005): Architectures of Laboratory-PC and Mobile Pocket PC Brain-Computer Interfaces. *Proceedings of the 2nd International IEEE EMBS Conference on Neural Engineering*, Arlington, Virginia, March 16 - 19.

Elidan J., Langhofer L., and Honrubia V. (1987): Recording of short-latency vestibular evoked potentials induced by acceleration impulses in experimental animals: current status of the method and its applications. *Electroencephalography and Clinical Neurophysiology*, vol. 68, pp. 58-69.

Elidan J., Leibner E., Freeman S., Sela M., Nitzan M., and Sohmer H. (1991): Short and middle latency vestibular evoked responses to acceleration in man. *Electroencephalography and clinical neurophysiology*, vol. 80, no. 2, pp. 140-145.

Elidan J., Sohmer H., Lev S., and Gay I. (1984): Short latency vestibular evoked response to acceleration stimuli recorded by skin electrodes. *The Annals of Otology, Rhinology, and Laryngology*, vol. 93, pp. 257-261.

Elidan J., Sohmer H., and Nizan M. (1982): Recording of short latency vestibular evoked potentials to acceleration in rats by means of skin electrodes. *Electroencephalography and Clinical Neurophysiology*, vol. 53, pp. 501-505.

Eoh H. J., Chung M. K., and Kim S. H. (2005): Electroencephalographic study of

drowsiness in simulated driving with sleep deprivation. *International Journal of Industrial Ergonomics*, vol. 35, pp. 307-320.

Gao X., Xu D., Cheng M., and Gao S. (2003): A BCI-Based Environmental Controller for the Motion-Disabled. *IEEE Transactions on Neural Systems and Rehabilitation Engineering*, vol. 11, no. 2, pp. 137-140.

Girolami M. (1998): An alternative perspective on adaptive independent component analysis. *Neural Computation*, vol.10, pp.2103–2114.

Groen E. L., Howard I. P., and Cheung B. S. (1999): Influence of body roll on visually induced sensation of self-tilt and rotation. *Perception*, vol. 28, pp. 287-297.

Guger C., Schlögl A., Neuper C., Walterspacher D., Strein T., and Pfurtscheller G. (2001): Rapid Prototyping of an EEG-Based Brain–Computer Interface (BCI). *IEEE Transactions on Neural Systems and Rehabilitation Engineering*, vol. 9, no. 1, pp. 49–58.

Jung T. P., Humphries C., Lee T. W., Makeig S., McKeown M. J., Iragui V., and Sejnowski T. J. (1998): Extended ICA removes artifacts from electroencephalographic recordings. *Advances in Neural Information Processing Systems*, vol. 10, pp. 894-900.

Jung T. P., Makeig S., Humphries C., Lee T. W., McKeown M. J., Iragui V., and Sejnowski T. J. (2000): Removing electroencephalographic artifacts by blind source separation. *Psychophysiology*, vol. 37, pp. 163-78.

Jung T. P., Makeig S., Stensmo M., and Sejnowski T. J. (1997): Estimating alertness from the EEG power spectrum. *IEEE Transactions on Biomedical Engineering*, vol. 44, no. 1, pp. 60–69.

Jung T. P., Makeig S., Westerfield W., Townsend J., Courchesne E., and Sejnowski T. J. (2001): Analysis and visualization of single-trial event-related potentials. *Human Brain Mapping*, vol. 14, no.3, pp. 166-185.

Jutten C. and Herault J. (1991): Blind separation of sources I. An adaptive algorithm based on neuromimetic architecture. *Signal Processing*, vol. 24, pp. 1-10.

Kalcher J., Flotzinger D., Neuper C., Gölly S., and Pfurtscheller G. (1996): Graz brain–computer interface II: Toward communication between humans and computers based on online classification of three different EEG patterns. *Medical and Biological Engineering and Computing*, vol. 34, no. 5, pp. 382–388.

Kemeny A. and Panerai F. (2003): Evaluating perception in driving simulation experiments. *Trends in Cognitive Sciences*, vol. 7, pp. 31-37.

Kobayashi T. and Takahashi K. (2003): Linux DSP Gateway Specification Rev2.0, *Nokia Corporation*, Nov. 13.

Lee T. W., Girolami M., and Sejnowski T. J. (1999): Independent component analysis using an extended infomax algorithm for mixed sub- and super-Gaussian sources. *Neural Computation*, vol.11, pp. 606-633.

Liao R., Krolik J. L., and McKeown M. J. (2005): An information-theoretic criterion for intrasubject alignment of FMRI time series: motion corrected independent component analysis. *IEEE Transactions on Medical Imaging*, vol. 24, no. 1, pp. 29-44.

Lin C. T., Ko L. W., Chung I. F., Huang T. Y., Chen Y. C., Jung T. P., and Liang S. F. (2006): Adaptive EEG-based Alertness Estimation System by Using ICA-based Fuzzy Neural Networks. *IEEE Transactions on Circuits and System I: Regular Papers*, vol. 53, no. 11, pp. 2469-2476.

Lin C. T., Wu R. C., Liang S. F., Chao W. H., Chen Y. J., and Jung T. P. (2005): EEG-based drowsiness estimation for safety driving using independent component analysis. *IEEE Transactions on Circuits and Systems I*, vol. 52, no. 12, pp. 2726 – 2738.

Lin C. T., Wu R. C., Jung T. P., Liang S. F., and Huang T. Y. (2005): Estimating Driving Performance Based on EEG Spectrum Analysis. *EURASIP Journal on Applied Signal Processing*, vol. 19, pp. 3165-3174.

Liu Jane W. S., *Real-Time Systems*, Prentice Hall Upper Saddle River, NJ, 2000.

Loose R., Probst T., Tucha O., Bablok E., Aschenbrenner S., and Lange K. W. (2002): Vestibular evoked potentials from the vertical semicircular canals in humans evoked by roll-axis rotation in microgravity and under 1-G. *Behavior Brain Research*, vol. 134, pp. 131-137.

Makeig S. (1993): Auditory event-related dynamics of the EEG spectrum and effects of exposure to tones. *Electroencephalography and Clinical Neurophysiology*, vol. 86, pp. 283-293.

Makeig S., Delorme A., Westerfield M., Jung T. P., Townsend J., Courchense E., and Sejnowski T. J. (2004): Electroencephalographic brain dynamics following visual targets requiring manual responses. *PLOS Biology*, vol. 2, no.6, pp. 747-762.

Makeig S. and Inlow M. (1993): Lapses in alertness: coherence of fluctuations in performance and EEG spectrum. *Electroencephalography and Clinical Neurophysiology*, vol. 86, no. 1, pp. 23–35.

Makeig S. and Jung T. P. (1995): Changes in alertness are a principal component of variance in the EEG spectrum. *Neuroreport*, vol. 7, no. 1, pp. 213–216.

Makeig S. and Jung T. P. (1996): Tonic, phasic, and transient EEG correlates of auditory awareness in drowsiness. *Cognitive Brain Research*, vol. 4, no. 1, pp. 15–25.

McGregor D. K. and Stern J. A. (1996): Time on task and blink effects on saccade duration. *Ergonomics*, vol. 39, pp. 649-660.

Merfeld D. M., Zupan L., and Peterka R. J. (1999): Humans use internal models to

estimate gravity and linear acceleration. *Nature*, vol. 398, pp. 615-618.

Naganawa M., Kimura Y., Ishii K., Oda K., Ishiwata K., and Matani A. (2005): Extraction of a plasma time-activity curve from dynamic brain pet images based on independent component analysis. *IEEE Transactions on Biomedical Engineering*, vol. 52, no. 2, pp. 201–210.

NHTSA. *National Highway Traffic Safety Administration*, Washington, DC. Drowsy driver detection and warning system for commercial vehicle drivers: Field proportional test design, analysis, and progress. [Online] Available: http://www.nhtsa.dot.gov/

NSF. *National Sleep Foundation*, Washington, DC. Sleep facts and stats. [Online] Available: http://www.sleepfoundation.org/

Obeid I., Nicolelis M., and Wolf P. (2004): A multichannel telemetry system for signal unit neural recording. *Journal of Neuroscience Methods*, vol. 133, no. 2, pp. 33-38.

Obermaier B., Neuper C., Guger C., and Pfurtscheller G. (2001): Information transfer rate in a five-classes brain-computer interface. *IEEE Transactions on Neural Systems and Rehabilitation Engineering*, vol. 9, no. 3, pp. 283-288.

Orden K. V., Jung T. P., and Makeig S. (2000): Combined eye activity measures accurately estimate changes in sustained visual task performance. *Biological Psychology*, vol. 52, no. 3, pp. 221-40.

Orden K. V., Limbert W., Makeig S., and Jung T. P. (2001): Eye activity correlates of workload during a visualspatial memory task. *Human Factors*, vol. 43, no. 1, pp. 111-121.

Page N. G., and Gresty M. A. (1985): Motorist's vestibular disorientation syndrome. *Journal of Neurology, Neurosurgery & Psychiatry*, vol. 48, pp. 729-735.

Parker D. E. and Phillips J. O. (2001): Self-motion perception: assessment by

real-time computer-generated animations. *Applied Ergonomics*, vol. 32, pp. 31-38.

Piccini L., Arnone L., Beverina F., Cucchi A., Petrelli L., and Andreoni G. (2004): Wireless DSP architecture for biosignals recording. *Proceedings of the 4th IEEE International Symposium on Signal Processing and Information Technology*, pp. 487- 490, Dec. 18-21.

Pilutti T. and Ulsoy G., (1999): Identification of Driver State for Lane-Keeping Tasks. *IEEE Transactions on Systems, Man and Cybernetics, Part A: Systems and Humans*, vol. 29, pp. 486-502.

Polich J. and Comerchero M. (2003): P3a from visual stimuli: typicality, task, and topography. *Brain Topography*, vol. 15, pp. 141-152.

Probst T., Ayan T., Loose R., and Skrandies W. (1997): Electrophysiological evidence for direction-specific rotary evoked potentials in human subjects -- a topographical study. *Neuroscience letters*, vol. 239, pp. 97-100.

Probst T., Bablok E., Dabrowski H., Dombrowski J. H., Loose R., and Wist E. R. (1996): Position and velocity responses from the otoliths and the canals: results from ESA's parabolic flights. *Aviation, space, and environmental medicine*, vol. 67, no. 7, pp. 633-639.

Probst T., Dabrowski H., Liebler G., and Wist E. R. (1993): MARDER -- Multi-Axes Rotation Device for Experimental Research: a new concept for investigations of the vestibular, oculomotor, and visual systems of humans in three-dimensional space. *Journal of neuroscience methods*, vol. 49, pp. 49-61.

Reymond G. and Kemeny A. (2000): Motion cueing in the Renault driving simulator. *Vehicle System Dynamics*, vol. 34, pp. 249-259.

Reymond G., Kemeny A., Droulez J., and Berthoz A. (2001): Role of lateral acceleration in curve driving: driver model and experiments on a real vehicle and

a driving simulator. *Human Factors*, vol. 43, pp. 483-495.

Roberts S., Rezek I., Everson R., Stone H., Wilson S., and Alford C. (2000): Automated assessment of vigilance using committees of radial basis function analysers," *IEE Science Measurement and Technology*, vol. 147, pp. 333–338.

Seidmann S. H., Telford L., Paige G. D. (1998): Tilt perception during dynamic linear acceleration. *Experimental Brain Research*, vol. 119, pp. 307-314.

Sterlade M. (1993): Central Core Modulation of Spontaneous Oscillations and Sensory Transmission in Thalamocortical Systems. *Current Opinion in Neurobiology*, vol. 3, no.4, pp. 619-625.

Stern J. A., Boyer D., and Schroeder D. (1994): Blink rate: Possible measure of fatigue. *Human Factors*, vol. 36, pp. 285-297.

Stewart D. (1965): A platform with six degrees of freedom. *Institution of Mechanical Engineers, Proceedings*, vol. 180, pp. 371–386.

Thakor N. V. (1999): *Biopotentials and Electro-physiology Measurement*. The Measurement, Instrumentation and Sensors Handbook, J. H. School of Medicine.

Thilo K. V., Kleinschmidt A., and Gresty M. A. (2003): Perception of self-motion from peripheral optokinetic stimulation suppresses visual evoked responses to central stimuli. *Journal of Neurophysiology*, vol. 90, pp. 723-730.

Treisman M. (1984): Temporal Rhythms and Cerebral Rhythms. *Annals of the New York Academy of Sciences*, vol. 423, pp. 542-565.

Vuckovic A., Radivojevic V., Chen A. C. N., and Popovic D. (2002): Automatic recognition of alertness and drowsiness from EEG by an artificial neural network. Medical engineering & physics, vol. 24, pp. 349-360.

Wexler M., Lamouret I., and Droulez J. (2001): The stationarity hypothesis: an allocentric criterion in visual perception. *Vision Research*, vol. 41, pp. 3023-3037.

Whitchurch A. K., Ashok B. H., Kumaar R. V., Sarukesi K., and Varadan V. K. (2002): Wireless system for long term EEG monitoring of Absence Epilepsy. *Biomedical Applications of Micro- and Nanoengineering*, vol. 4937, pp. 343-349.